Novel tetradentate N_2O_2 water-soluble Schiff Base and its Al(III) complex: synthesis, structural characterization, and correlations between structure and stability against hydrolysis

Hajer Bouznif[1,2,*], Licínia L. G. Justino[2,*], Maria I. L. Soares[2], Telma Costa[2], M. Luísa Ramos[2], Timur Nikitin[2], Teresa M. V. D. Pinho e Melo[2], Nabil Zouari[1] and Rui Fausto[2,3]

[1] *Laboratory Physico-Chemistry of the Solid State, Department of Chemistry, Faculty of Sciences of Sfax, B. P. 1171, Sfax 3000, University of Sfax, Tunisia*

[2] *CQC-IMS, Department of Chemistry, University of Coimbra, Rua Larga 3004-535 Coimbra, Portugal*

[3] *Faculty of Sciences and Letters, Department of Physics, Istanbul Kultur University, Ataköy Campus, Bakirköy 34156, Istanbul, Turkey*

Abstract

A novel water-soluble di-Schiff base, *N,N'*-bis(3-methoxy-5-sulfonatosalicylidene)-1,2-ethylenediamine disodium salt (**MSS**), was synthesized under both conventional heating and microwave-assisted conditions. Detailed characterization was conducted using various techniques including NMR, HRMS, UV–vis, SEM/EDX, DSC, ATR-FTIR and Raman spectroscopies, accompanied by DFT calculations. The study discusses the enol-imine/keto-enamine tautomerism of **MSS** based on theoretical, solution and solid-state results, as well as the impact of intra- and intermolecular interactions on the balance between the tautomers. The enol-imine form was predicted as the most stable tautomer in gas phase. Nonetheless, the keto-enamine form was found to be the main tautomer in water, DMSO and in the solid state. To assess the stability of **MSS** and to study its complexation with Al(III) in aqueous and non-aqueous media, a combined spectroscopic and computational approach was used. The stability of **MSS** against hydrolysis was analyzed and compared with that of its non-substituted analogue. The differences found were interpreted based on the different tautomeric equilibria of the two Schiff bases and specific structural susceptibilities towards nucleophilic attack by water. The presented results impact on the development of more efficient strategies for the design of water-stable Schiff bases, highlighting the role of tautomerism in determining stability against hydrolysis. NMR data revealed the formation of a stable Al(III) complex with **MSS** and additional complexes with **MSS** degradation products in the pH range 4–7. The infrared and Raman results provided additional structural details and supported the aforesaid conclusions.

Keywords : Water soluble Schiff base, enol-imine (O-H···N) // keto-enamine (O···H-N), Hydrolysis, Al(III) complex, DFT calculations.

Corresponding authors e-mails: bouznifhajer13@gmail.com (Hajer Bouznif), liciniaj@ci.uc.pt (Licínia L. G. Justino)

Introduction

Schiff bases were initially synthesized by Hugo Schiff in 1864 [1], and are among the most commonly utilized organic compounds. They are still an intriguing topic that fascinates many research groups around the world, and due to their versatility, stability and broad spectrum of applications, they are considered “privileged ligands” [2,3].

These compounds are characterized by an imine (-C=N-) functional group and are usually prepared through condensation of aldehydes or ketones with primary amines [1]. Their development was a significant step forward in coordination chemistry [4,5] and their applications involve many areas, such as catalysis [6], solar energy applications [6], optical chemical sensors [7], LED applications [8], renewable energy materials [9], medicinal chemistry [10] and others.

Among these, the N,N′-ethylenebis(salicylimine) (salen) chelating double Schiff base and its derivatives are likely among the most extensively studied compounds [11,12]. Even though the first metal salen complex was described by Pfeiffer et al. in 1933 [13], due to their simplicity in synthesis, synthetic adaptability, kinetic and thermodynamic stability and the presence in their structure of a potential O,N,N,O donor atom set for tetradentate coordination, there is an ongoing scientific interest in studying their strong affinity to coordinate with many metal ions by precise arrangement of the imine and hydroxyl groups [3,12,14–21]. The review by Andrea et al. provides a comprehensive discussion of the versatility of aluminum Salen complexes in facilitating highly selective transformations in stereoselective catalysis. This review emphasizes the critical role of the tunable electronic and steric properties of Salen ligands, which made them particularly effective in asymmetric reactions. [20]

The synthesis of Schiff base complexes with earth abundant metals is particularly relevant for their use in large scale applications, since using these metals is more sustainable and cost-effective compared to precious metals. In this context, aluminium is a convenient metal since it is ubiquitous in the environment (it is the most prevalent element after silicon and oxygen in the Earth’s crust, accounting for more than 8% of its mass), and is relatively non-toxic compared to other metals. Due to its high availability, aluminum and its alloys are frequently used for many applications [20,22–24]. For example, aluminum compounds are efficient Lewis acid catalysts and are utilized in a variety of catalytic processes, including copolymerization, CO_2 insertion reactions, hydroamination, and hydroboration [25], and have proven their potential in both homogeneous and heterogeneous catalysis [26].

There is an increasing demand to use metal salen complexes in aqueous systems due to the current upswing in various fields such as catalysis [27]. However, this is frequently hampered by the complexes' insolubility in water. Thus, attaching highly polar substituents or hydrophilic groups (such as sulfonates, carboxylates, phosphates, or sulfates) to salen ligands could be a solution to this issue. Nevertheless,

several investigations have concluded that this type of compounds show a tendency to undergo hydrolytic cleavage of the azomethine linkages, which limit its uses [15,28,29]. Hence, the investigation of the hydrolysis process of water-soluble Schiff bases and of their complexation in aqueous solution remain topics of high interest.

Tautomerism is a significant occurrence in biochemistry [30–32], and synthetic chemistry [33–36]. The salen Schiff bases, in which the OH group is *ortho* to −HC=N, are of considerable interest, since these compounds are well-known to usually undergo easy enol-imine/ keto-enamine tautomerism [37,38]. The ability to remotely influence this equilibrium by using different substituents to control the concentration of the enol or keto tautomers presents an interesting challenge and has implications that go beyond the potential applications related with each tautomer, as this equilibrium and the intrinsic reactivity of each tautomer determine the global stability of the Schiff base against hydrolysis, as demonstrated in this paper.

In this manuscript we have also explored the use of microwave-assisted synthesis, and compared its effectiveness with conventional synthetic methods, as this strategy is becoming a key aspect of green chemistry. We have, thus, synthesized a water-soluble di-Schiff base *N,N'*-bis(3-methoxy-5-sulfonatosalicylidene)-1,2-ethylenediamine disodium salt (abbreviated as **MSS**), which was subsequently employed in complexation studies in aqueous solution and to synthesize a novel Al(III) complex in non-aqueous media. We were particularly interested in investigating the effect of the methoxy substituent in the stability and in the keto/enol tautomeric equilibrium of the Schiff base. Furthermore, we performed a thorough speciation and structural characterization study of the complexes formed in the Al(III)/MSS system in aqueous solution and compared them to the synthesized complex in non-aqueous media. The structural characterization of the complexes was performed in solution using NMR and in the solid-state using Raman and infrared spectroscopies, together with SEM/EDX and DSC, and these studies were supplemented with density functional theory (DFT) calculations.

Results and discussion

1. *Synthesis and characterization of the ligand **MSS***

The new water-soluble di-Schiff base *N,N'*-bis(3-methoxy-5-sulfonatosalicylidene)-1,2-ethylenediamine disodium salt (**MSS**) was synthesized by a four-step sequence as outlined in Scheme I following a procedure adapted from the literature [39]. The final step of the sequence involves the condensation of sodium 3-methoxy-salicylaldehyde-5-sulfonate 5-S-3-OMe and 1,2-ethylenediamine in a molar ratio of 2:1. The reaction can be carried out under conventional heating or microwave-assisted

conditions, and we concluded that microwave irradiation resulted in a faster and more efficient synthesis of the Schiff base (Table S1), besides requiring less solvent than the conventional technique. The structure of the ligand **MSS** was confirmed by ^{1}H and ^{13}C NMR spectroscopy and HRMS (Figures S1 and S2). In addition, its high melting point (mp > 300 ºC) confirms the presence of the sodium sulfonate ionic groups [40]. **MSS** exhibits significant solubility in H_2O and in organic solvents with high polarity such as DMSO and DMF. On the other hand, it is only slightly soluble in less polar organic solvents such as chloroform, tetrahydrofuran (THF), 1,4-dioxane, and n-hexane.

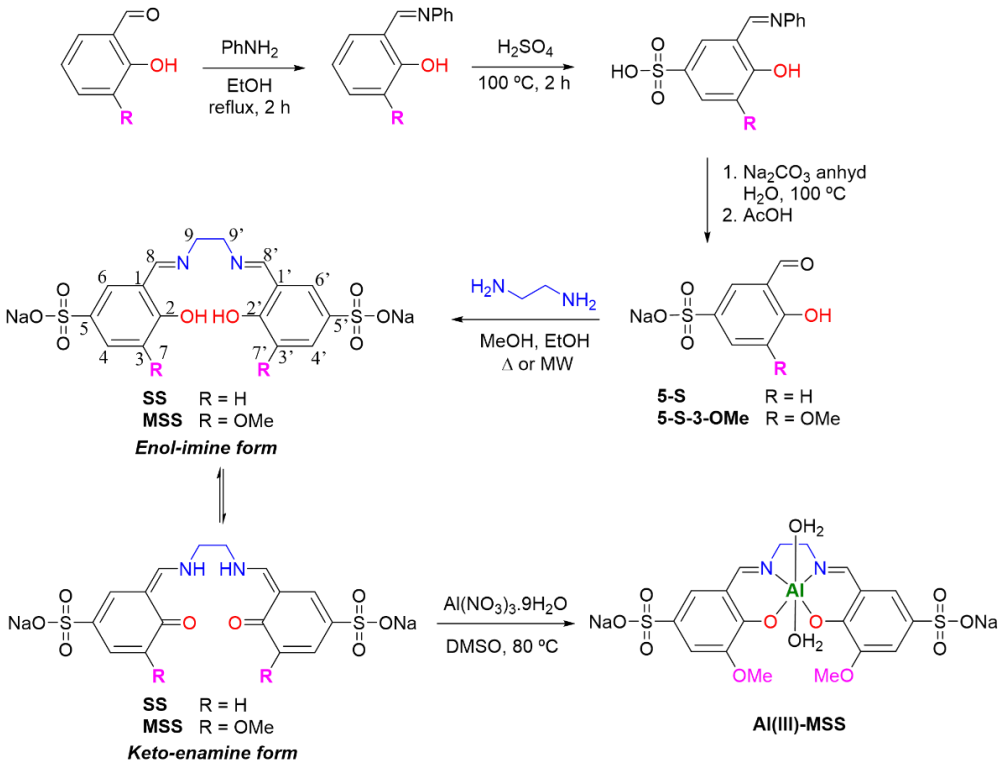

Scheme I: Synthetic route to water-soluble sulfonato-salen-type ligands **SS** and **MSS**, and **Al(III) / MSS** complex.

*1.1. Structure and energetics of **MSS***

MSS (Scheme I) is composed of two aryl rings, with two hydroxyl groups at the C-2 and C-2' positions, two sulfonate groups at positions C-5 and C-5' and two methoxy groups at positions C-7 and C-7'. Besides exhibiting keto–enol type tautomerism (enol-imine / keto-enamine equilibrium), **MSS** may also exist in several conformational forms differing by rotation around the C9-C9', C9-N, C1-C8 and C5-S bonds, and/or conformations of the methoxy and hydroxy substituents of the six-membered rings.

To help understanding the structure of **MSS** in solution and in the solid-state, we have carried out computational studies on the different possible forms of the compound, paying particular attention to their relevance for the tautomerism. After a preliminary molecular mechanics thorough conformational search,

the different species were optimized at the DFT(B3LYP)/6–311++G(d,p) level in gas phase (isolated molecule in vacuum), and also in water and DMSO. The structural and energetic results are presented in Figures 1 and S3, as well as in Tables 1, S2 and S3.

The C_2 symmetry keto form I-b-NH (Figure 1), with two strong intramolecular hydrogen bonds, with N–H···O distance of 1.795Å, was found to be the most stable form in water, as well as in DMSO, with an estimated population of ca. 67% at 298.15 K. The keto-enamine conformers II-c-NH, IV-a-NH, VI-d-NH, and the enol-imine forms III-c-OH, V-b-OH, VII-d-OH, VIII-a-OH (Figures 1 and S3), also present two intramolecular hydrogen bonds, with N–H···O and OH···N distances close to 1.799 and 1.682 Å, respectively. Although their hydrogen bonds are relatively strong, these structures are significantly less stable than form I-b-NH, with ΔG^o values of 1.9–21.2 kJ/mol relative to this species. Interestingly, the conformer of the enol form presenting a hydrogen bond between the OH donor group and the methoxy oxygen was found to have a high energy (66.3 kJ/mol, Figure S3). In accordance with these results, the UV-vis absorption spectrum obtained for **MSS** in water (Figure 2(a)) immediately after sample preparation shows a band at 406 nm, which indicates [41,42] the presence of the keto-enamine tautomer in solution. These results are also in agreement with previous investigations that have shown that the keto-enamine form is favored in polar solvents, in some cases becoming the dominant form [37,43,44], as a consequence of its higher dipolar character [45].

On the other hand, for the isolated molecule the enol form VIII-a-OH is predicted as the most stable species. The higher stability of the isolated enol form may be attributed to the presence in this form of a strong OH···N hydrogen bond and, with all probability, also to a higher aromaticity of the six-membered rings in their phenolic configuration, which is partially lost in the keto-enamine species. It should be mentioned that the influence of the Na^+ ion was not considered in these calculations, as the ion pair is expected to be dissociated in solution. The gas phase calculations were intended for comparative purposes, and therefore were performed for the same molecular models.

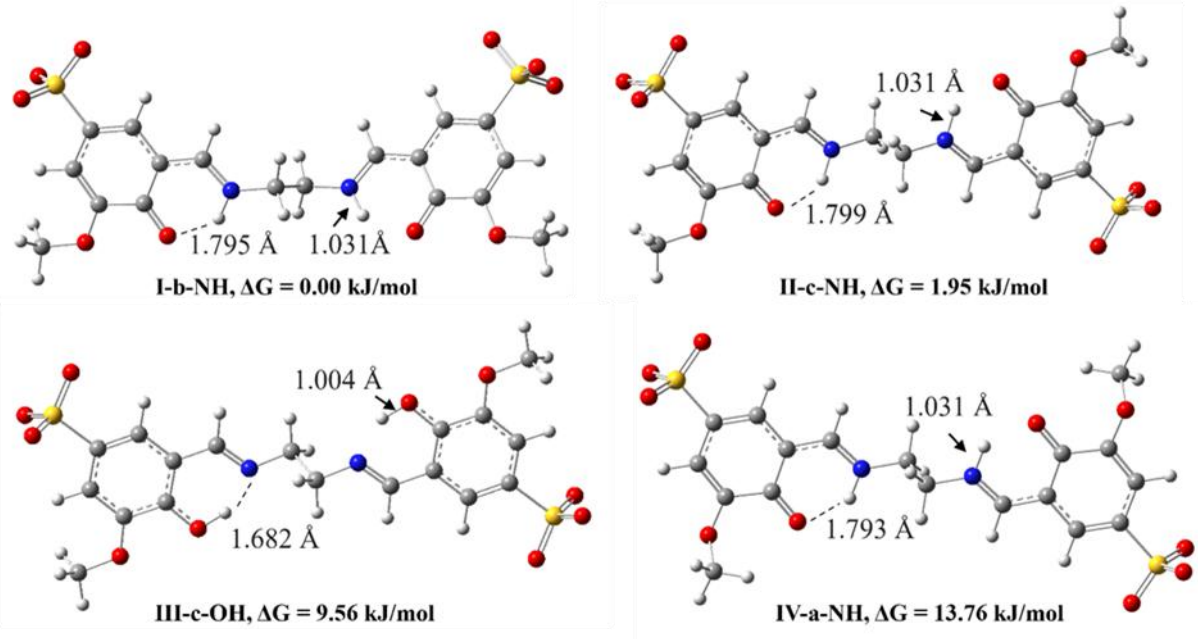

Figure 1. DFT(B3LYP)/6–311++G(d,p) optimized geometries of the most stable conformers and tautomers of *N*,*N*'-bis(3-methoxy-5-sulfonatosalicylidene)-1,2-ethylenediamine (**MSS**), considering the bulk effects of water solvent (the numbering of the conformers/tautomers from **I** to **IV** follows the order of their decreasing relative stability and population in water. The letters from **a** to **c** are related to the conformational arrangement of the conformer).

Table 1. DFT(B3LYP)/6–311++G(d,p) calculated relative electronic energies (ΔE_{el}) (kJ mol^{-1}), zero-point-corrected electronic energies (ΔE_{Total}), Gibbs energies at 298.15 K ($\Delta G°_{298K}$), and equilibrium populations (%) (P_{298}) estimated from the relative Gibbs energies of the lowest energy conformers and tautomers of **MSS**, considering the bulk effects of water solvent.

Structure	**I-b-NH**	**II-c-NH**	**III-c-OH**	**IV-a-NH**	**V-b-OH**	**VI-d-NH**	**VII-d-OH**	**VIII-a-OH**
Symmetry	C_2	C_i	C_i	C_i	C_2	C_i	C_1	C_i
ΔE_{el} (kJ/mol)	0.0	0.0	10.5	18.9	9.8	18.9	28.5	28.4
$\Delta(E_{total})$ (kJ/mol)	0.0	0.4	6.5	15.9	6.2	16.2	21.4	21.6
$\Delta G°_{298k}$	0.0	2.0	9.6	13.8	14.4	15.1	16.9	21.2
P_{298} (%)	67.2	30.6	1.4	0.3	0.2	0.2	0.1	0.0

1.2. Schiff base stability in aqueous solution

In our efforts to synthesize the Schiff base **MSS**, the initial attempts in the presence of water proved to be unsuccessful, likely due to the high susceptibility of the imine groups to hydrolysis. To help clarify our observations, the non-substituted compound *N,N'*-bis(5-sulfonatosalicylidene)-1,2-ethylenediamine disodium salt (**SS**) was synthesized to allow evaluation of the influence of the electron-

donating methoxy group present in **MSS** on the hydrolysis process (Scheme I). Herein, we conducted UV–vis experiments to quantify the rate of this hydrolytic reaction at pH close to 7.

At the outset, we examined the UV–vis spectra of the aldehyde precursors **5-S** and **5-S-3-OMe** (Scheme I) in water to evaluate their stability. Our findings confirmed their long-term stability in water over a period exceeding one week. Subsequently, we investigated the UV–vis spectra of **MSS** and **SS** in water over time (Figure 2). Immediately after solution preparation, the spectra of **MSS** and **SS** exhibited distinct features, with absorption maxima observed at 248, 292, and 406 nm, and at 224, 236, 274, 316, and 388 nm. These spectra are notably different from those of their aldehyde precursors. Compared to unsubstituted **SS**, the absorption maxima of **MSS** are red-shifted due to insertion of the electron donor methoxy group. However, within a short period of time, the spectrum of **MSS** underwent a gradual transformation, converging into its final form (maxima at 247 and 377 nm), almost overlapping that of **5-S-3-OMe**. Along the same period, the **SS** absorption spectrum converged also towards its final form, with maxima at 222, 236, 255, 322 and 377 nm. Only three bands overlapped with those in the spectrum of **5-S** (maxima at 222, 255, 322 nm), suggesting a slower hydrolysis process for the non-substituted Schiff base. The obtained results suggest that the presence of a *meta* methoxy group makes the Schiff base more prone to hydrolysis (in neutral medium) compared to its non-substituted analogue.

Note that the analysis of the effect of the methoxy group in *meta* position is not straightforward since, besides an inductive electron-withdrawing effect, the methoxy group also exerts an electron-donating effect through resonance, which is, however, less pronounced in the *meta* position compared to the *ortho* and *para* positions. To rationalize these results, the Mulliken charges on the imine carbons of the most stable conformers of both **MSS** and **SS** were calculated by DFT. Inspection of these charges provided additional insight regarding their resistance towards hydrolysis. The charge of the imine carbon of the most stable conformer of **MSS** (I-b-NH, with 67.2% population) is +0.205 *e* (Table S4), while the charges on the imine carbons of the dominant conformers of **SS** are negative, namely –0.034 *e* (VI-d-NH, 50.6% population), and –0.067 *e* (VIII-a-OH, 32.6% population) (Table S4). A more positive charge on the imine carbon indicates that the carbon is more electrophilic and can make the Schiff base more susceptible to nucleophilic attack by water, leading to hydrolysis. The differences in the tautomeric equilibria of the two Schiff bases, together with the different susceptibilities of their structures towards nucleophilic attack by water, ultimately lead to the observed slower hydrolysis of **SS**.

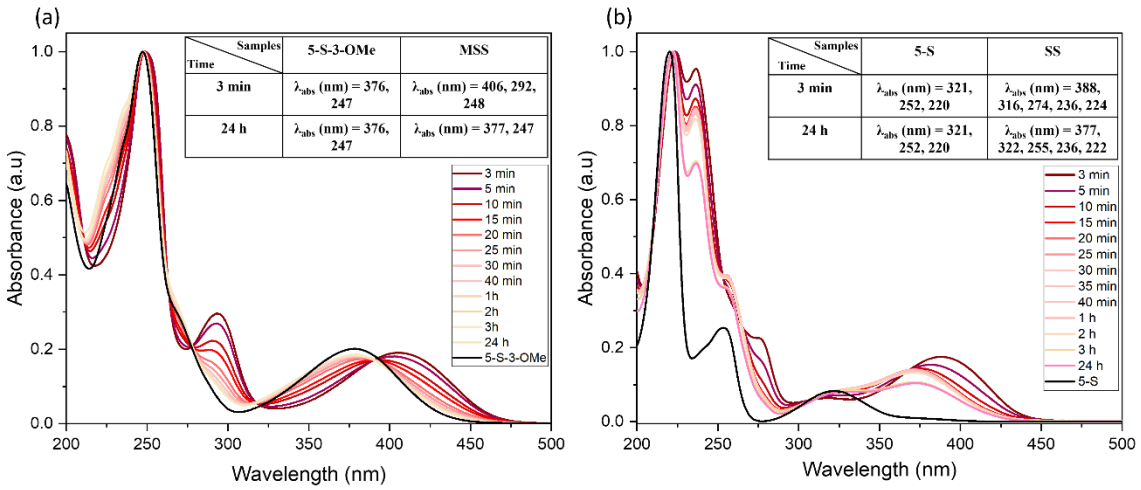

Figure 2. Normalized absorption spectra of (a) the aldehyde **5-S-3-OMe** and the Schiff base **MSS** (pH 7.4) and (b) of the aldehyde **5-S** and the Schiff base **SS** (pH 7.2) in H_2O at room temperature.

To gain further insights on the stability of **MSS** in more concentrated solutions (~5 mmol dm^{-3}), a series of NMR measurements in D_2O were carried out over time. The ^1H NMR spectra after 24 h exhibit remarkable variation compared to the first one (3 min), and it is more complex than expected, revealing the formation of several hydrolytic species. Further investigations were conducted, and these findings will be presented in Section 2.1. The instability of **MSS** at low pH was not surprising given that the reaction is catalysed by acidic media. Surprisingly, the unexpected hydrolysis of **MSS** under conditions approximating neutrality indicated that acid catalysis is not required, as partial decomposition of the ligand into its precursor compounds and additional species is observed in these conditions.

The **MSS** molecule comprises two imine groups, known to be susceptible to hydrolysis under specific conditions, and previous reports indicate that the process of hydrolysis could potentially yield either mono-Schiff base or diol compounds, in addition to the precursor compounds.[15,29] To elucidate whether the hydrolysis of the **MSS** compound culminated in the formation of the mono-Schiff base or the diol (Figure S4), the NMR spectra of **MSS**, of the *N,N'*-mono(3-methoxy-5-sulfonatosalicylidene)-1,2-ethylenediamine monosodium salt (**m-MSS**), and of sodium 3-(dihydroxymethyl)-4-hydroxy-5-methoxybenzenesulfonate (**diol**) were simulated by DFT. The assignments are given in Table S5 and Figure S5 and are based on the B3LYP/GIAO calculation of the shielding constants of the compounds in water. Careful analysis allowed assignment of the different signals obtained in the experimental NMR spectra and showed that **MSS** hydrolysis creates largely the mono-Schiff base **m-MSS** (Figure S5), as will be explained in the following section.

2. *Complexation of **MSS** with Al(III)*

In view of previous reports demonstrating the successful formation of metal complexes with water-soluble Schiff bases [29,42,46,47], we decided to investigate the complexation of **MSS** with Al(III). In these studies, NMR spectrometry was used as the main technique for the studies in solution. As shown below, the results revealed the formation of a stable Al(III) complex with **MSS** and additional complexes with its degradation products in the pH range 4–7. The only complex detected at pH 4 was the 1:2 species $[Al(5\text{-}S\text{-}3\text{-}OMe)_2(H_2O)_2]^-$, while at pH 7 both the 1:2 $[Al(m\text{-}MSS)_2(H_2O)_2]^-$ and the 1:1 $[Al(MSS)(H_2O)_2]^-$ complexes were formed. The NMR data were also used to help identify the species constituting the solid **Al(III)/MSS** product synthesized in non-aqueous media (DMSO; see the Experimental part) and further characterized by SEM/EDX, DSC, as well as by Raman and infrared spectroscopy.

2.1. *Multinuclear NMR studies*

Schemes II, III and IV show the structures and numbering, for assignment purposes, of the water-soluble Schiff base **MSS** and the related compounds **5-S-3-OMe** and **m-MSS**, respectively.

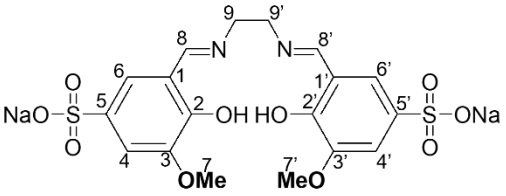

Scheme II

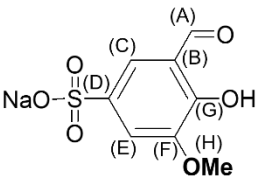

Scheme III

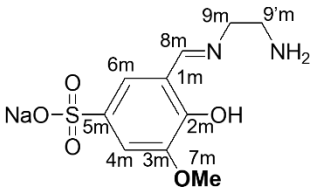

Scheme IV

For a complete structural characterization of the interaction of Al(III) metal ions with the water-soluble Schiff base **MSS**, (Scheme II) we have used a combination of ^{1}H and ^{27}Al NMR spectra at pH* values 4 and 7. Due to difficulties associated with the low abundance of the ^{13}C isotope and the low concentration of the complexed species, the ^{13}C NMR spectra are not provided for this system as the signal/noise ratio was not sufficient to easily detect all signals. Hydrolysis of Al(III) is observed at both pH 4 and 7, but becomes increasingly prominent at lower pH values. This competes with complexation, leading to the formation of hydrolytic Al(III) species. In addition to the information from ^{1}H chemical shifts, the ^{27}Al NMR spectra provide valuable structural details, including the type of metal centre present in these complexes, from the characteristic chemical shift and the symmetry around the metal centre from the spectral linewidth [48–54]. Generally, in aqueous solution, octahedral coordinated Al(III) is observed from −10 to around 50 ppm and tetrahedral coordinated Al(III) from around 60 to 80 ppm [48,52].

Intermediate chemical shifts have been assigned to five-coordinated Al(III) species [53,54]. ^{27}Al linewidths may vary from 3 Hz to several kHz, while the signal may even completely vanish into the baseline noise in some instances. This negative aspect of quadrupolar relaxation is counterbalanced by the additional information obtained concerning molecular symmetries from the magnitude of quadrupolar line broadenings and the favorable large range of ^{27}Al NMR chemical shifts, which is about 450 ppm.

Figure 3 shows a series of ^{1}H NMR spectra of aqueous solutions of the ligand (**MSS**) alone, at different conditions (Figures 3(a), (d) and (e)) and in the presence of aluminium nitrate (Figures 3(b), (c), (f) and (g)). Additionally, Figure 3(h) shows the ^{1}H NMR spectrum of an aqueous solution of the **Al(III) / MSS** complex (synthesized in DMSO). The corresponding ^{27}Al NMR spectra are shown in Figure 4, using the ^{27}Al NMR signal of $Al(NO_3)_3$ as external reference.

While the ligand **MSS** was found to be stable in organic solvents (DMSO, DMF), in aqueous solutions its ^{1}H NMR spectra in the absence of the Al^{3+} metal ion (Figures 3 (a), (d) and (e)) are quite complex, showing, in addition to the signals from the intact **MSS** ligand, new signals due to its degradation products. In acidic solutions (pH 4), the degradation is complete, as indicated by the absence of signals from **MSS** and, instead, rapid hydrolysis reactions result in the production of a large quantity of **5-S-3-OMe** (Scheme III) and ethylenediamine, precursors of the Schiff base **MSS**, and also minor quantities of an additional degradation product, identified on the basis of DFT calculations as the mono-Schiff base **m-MSS** (discussed in section 1.2), product of partial hydrolysis of **MSS** (Scheme IV). However, at higher pH values (pH 7), the degradation is far from complete. In addition to the ^{1}H NMR signals of **5-S-3-OMe** and ethylenediamine, we also detect the corresponding signals of the ligand **MSS** and of **m-MSS**. Similar results on the degradation of water-soluble Schiff bases were found in previous publications [15,29]. In fact, salen Schiff bases with the azomethine and hydroxy groups in adjacent positions have been shown to form an internal hydrogen bond, and the stability of the six-membered ring created by such an interaction can lead to increased stability of the Schiff base molecule [29]. However, this hydrogen bond can also activate the imine to undergo hydrolysis. Furthermore, a comparison of Figures 3(d) and 3(e) with Figure 3(a) suggests that both the intact ligand and the mono-Schiff base show greater stability in neutral solutions than in acidic medium. In addition, these results also indicate that **MSS** exhibits greater stability in more concentrated solutions, such as those used in the NMR studies. This is evident when compared to the hydrolysis process observed using UV–vis at the same pH and over the same period, which was conducted in a solution approximately 100 times more dilute.

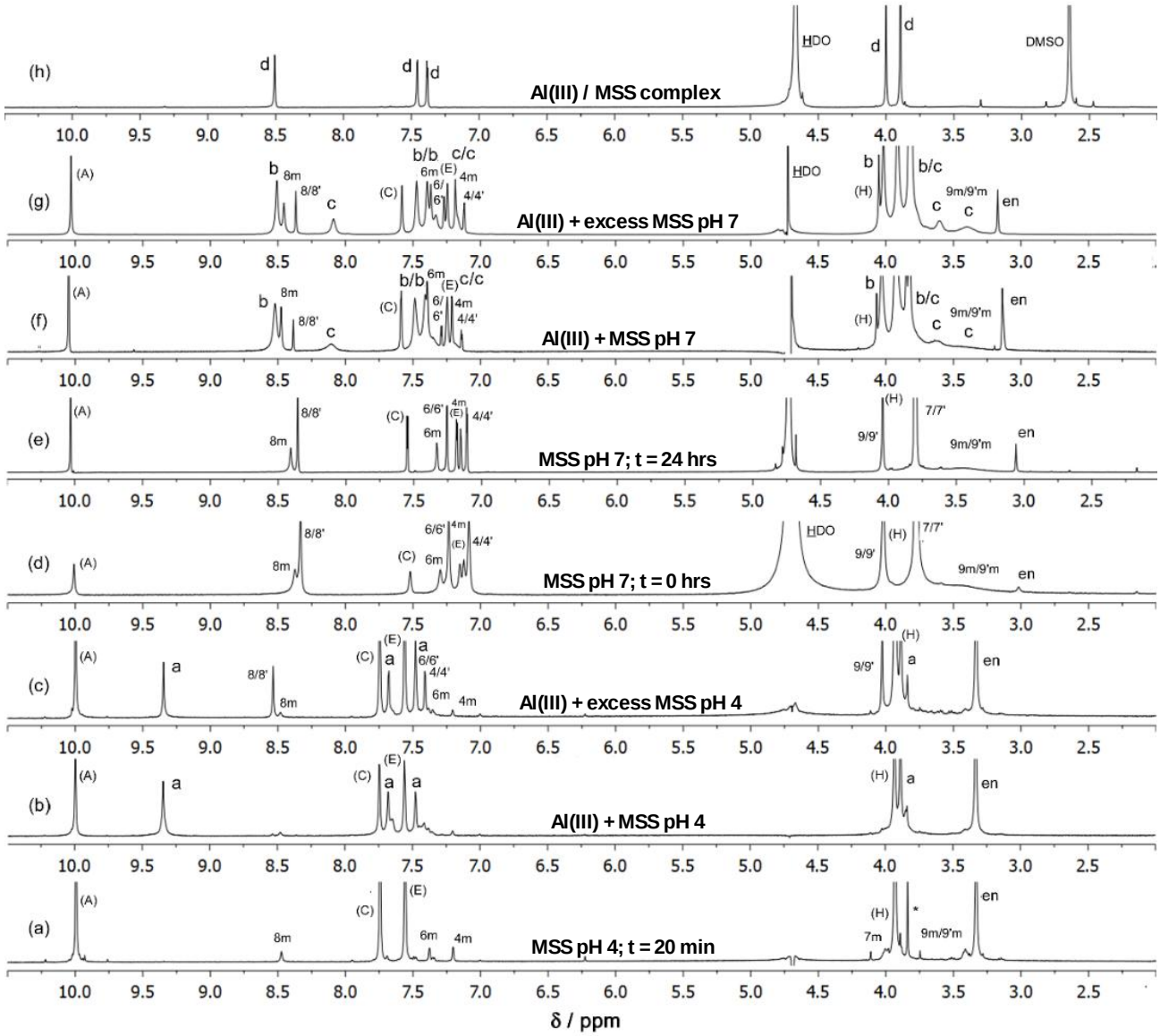

Figure 3. ^{1}H NMR spectra of solutions in D_2O of: (a) **MSS** 5.0 mmol dm^{-3}, pH* 4.03, 20 min after the dissolution; (b) **Al(III) / MSS** 5.0:5.0 mmol dm^{-3}, pH* 4.10; (c) **Al(III) / MSS** 2.5:5.0 mmol dm^{-3}, pH* 4.18; (d) **MSS** 5.0 mmol dm^{-3}, pH* of dissolution (pH* 7.00); (e) **MSS** 5.0 mmol dm^{-3}, 24 h after sample preparation; (f) **Al(III) / MSS** 5.0:5.0 mmol dm^{-3}, pH* 7.13; (g) **Al(III) / MSS** 5.0:10 mmol dm^{-3}, pH* 6.95 and (h) the **Al(III) / MSS** complex synthesized in DMSO, pH* 4.88; Temp. 298.15 K. *Signal not assigned.

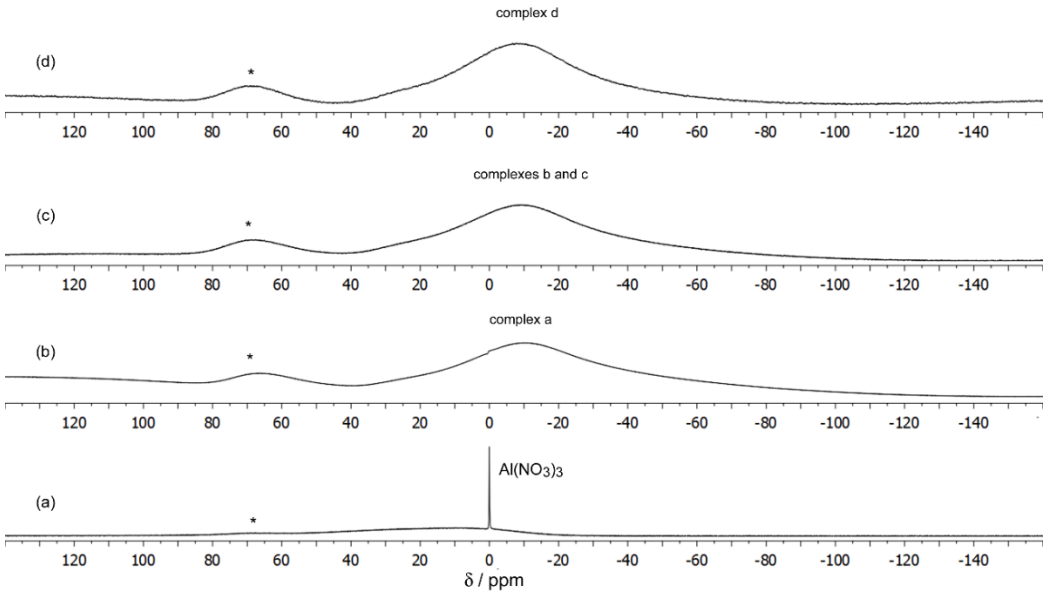

Figure 4. ^{27}Al NMR spectra of solutions in D_2O of (a) $Al(NO_3)_3$ 10 mmol dm^{-3}, pH* 2.0; (b) **Al(III) / MSS** 5.0:5.0 mmol dm^{-3}, pH* 4.10; (c) **Al(III) / MSS** 5.0:5.0 mmol dm^{-3}, pH* 7.13; (d) the **Al(III) / MSS** complex synthesized in DMSO, pH* 4.88; *Signal due to the aluminium of the probe.

Mixtures of aluminium nitrate and **MSS**, in aqueous solution, show additional ^{1}H signals due to complexed forms, depending on pH and molar ratios, in addition to those of any free intact ligand (**MSS**), and to the degradation products. Figures 3 (b), (c), (f) and (g) show a series of ^{1}H NMR spectra of the ligand in the presence of aluminium nitrate, where three complexes, **a, b,** and **c** are detected. The observation of distinct signals for free and complexed ligands in the ^{1}H NMR spectra suggests that free and complexed ligands are in slow exchange on the NMR time scale, for this system. Furthermore, as is shown in Figure 4, each of the complexes gives rise to a very broad ^{27}Al NMR signal ($\Delta\nu_{1/2} \approx 5.4$ KHz), with comparable chemical shift (δ = -9.7 ppm), suggesting the presence of an octahedral center in all the complexed species, in addition to the free metal present, as is suggested by the shoulder, at 24 ppm. The large $\Delta\nu_{1/2}$ of the ^{27}Al signals is probably related with the asymmetry of the complexed ligands around the metal center. The broad resonance around 60 ppm is associated with the aluminium signal of the probe [51].

Whereas species **a** is the only complex detected at low pH values (pH ~ 4), species **b** and **c** appear at higher pH values (pH ~ 7). Concerning complex **a**, detected at low pH, there is strong evidence that Al(III) binds to **5-S-3-OMe**, as this is the dominant species in solution. Two molecules of **5-S-3-OMe** coordinate one mononuclear Al^{3+} metal center, through the aldehyde (A) and the deprotonated aromatic hydroxyl OH (G) groups, forming one six-coordinated near octahedral complex, with the remaining apical positions occupied by two coordinated water molecules, as is suggested by the coordination induced ^{1}H NMR shifts observed for the (A), (C) and (E) proton nuclei (Table 2) and the ^{27}Al NMR spectrum (Figure

4). This conclusion is supported by the DFT calculated ^{1}H chemical shifts for $[Al(5\text{-}S\text{-}3\text{-}OMe)_2(H_2O)_2]^-$ (complex **a**, Table S5, Figure S6). The observation of only one set of ^{1}H signals means that the two complexed ligand moieties are magnetically equivalent (i.e. they have the same ^{1}H chemical shifts) and indicates a symmetrical 1 : 2 complex.

Furthermore, each of the complexes **b** and **c** also gives rise to one set of ^{1}H signals. These signals in the ^{1}H NMR spectrum experience significant chemical shift changes upon complexation compared to the corresponding signals of the ligand and its decomposition products in the absence of the Al^{3+} metal ion, under the same conditions. The induced complexation shift patterns suggest that one mononuclear Al(III) octahedral metal center binds to one molecule of the ligand **MSS** and to two molecules of mono-Schiff base **m-MSS**, in species **b** and **c**, respectively.

Complex **b** is expected to have a 1 : 1 (metal : ligand) stoichiometry, $[Al(MSS)(H_2O)_2]^-$, since one molecule of the intact ligand **MSS**, which is tetradentate, coordinates one octahedral aluminium centre through the deprotonated OH groups (2 and 2') and the N atoms of the azomethine (imine) N=CH groups, as is suggested by the ^{1}H NMR significant coordination induced shifts for the azomethine (imine) (8/8') and aromatic (4/4' and 6/6') protons associated to **MSS** complexation with the Al^{3+} metal ion (Table 2). Two molecules of H_2O are coordinated to the remaining apical positions of the aluminium metal centre, as is suggested by the observed ^{27}Al NMR spectrum (Figure 4). The DFT calculated ^{1}H chemical shifts for $[Al(MSS)(H_2O)_2]^-$ (complex **b**, Table S5) are in agreement with this conclusion.

For complex **c**, also detected at high pH values, there is strong evidence that one mononuclear centre of Al^{3+} coordinates two molecules of **m-MSS** by the azomethine (imine) groups (8m) and the aromatic OH groups (2m), with the remaining positions bound to two molecules of H_2O, in a symmetrical manner, as is suggested by the ^{1}H NMR coordination induced shifts pattern together with the narrowing of the ^{1}H NMR signals associated to the decreased flexibility of the CH_2 (9m/9'm) groups in the presence of the Al(III) metal ion. Whereas in the absence of the metal, the two non-equivalent methylene groups (9m and 9'm) of the mono-Schiff base are involved in a fast exchange process, showing only one broad signal, they display two individual broad signals in the presence of the metal, due to a reduction in the exchange rate, owed to the decreased flexibility of the CH_2 (9m) group after the metal coordination by the imine group (8m). The observation of only one set of ^{1}H signals means that the two complexed ligand moieties are magnetically equivalent (i.e. they have the same ^{1}H chemical shift), and indicates a symmetrical 1 : 2 (metal: ligand) complex. Additional support comes from the ^{27}Al NMR spectra (Figure 4) and from the DFT calculated ^{1}H chemical shifts for $[Al(m\text{-}MSS)_2(H_2O)_2]^-$ (complex **c**, Table S5, Figure S6).

Finally, a comparison of the ^{1}H NMR spectra shown in Figure 3(h) (the same as in Figure S7) with the corresponding spectra displayed in Figures 3 (f) and 3 (g) strongly suggests that the synthesized complex (complex **d**) and complex **b** are the same species.

Table 2. ^{1}H NMR parameters[a] for **MSS**, **5-S-3-OMe**, **m-MSS** and their complexes with Al(III), in D_2O solutions (298 K).

MSS[b]	H-8/8'	H-6/6'	H-4/4'	H-9/9'	H-7/7'
pH* 4.0	8.50	7.41	7.23	4.03	3.92
pH* 7.0	8.37	7.30	7.12	4.02	3.80
5-S-3-OMe [b]	(A)	(C)	(E)	(H)	
pH* 4.0	9.99	7.74	7.56	3.93	
pH* 7.0	10.09	7.58	7.39	4.07	
m-MSS[b]	H-8m	H-6m	H-4m	H-9m/H-9'm	H-7m
pH* 4.0	8.47	7.38	7.20	3.43	3.81
pH* 7.0	8.45	7.37	7.19	3.40 (broad)	3.76
Complex a [c]	(A)	(C)	(E)	(H)	
pH* 4.0					
δ	9.34	7.66	7.47	3.89	
Δδ (**5-S-3-OMe**)	-0.65	-0.08	0.08	-0.04	
Complex b [c]	H-8/8'	H-6/6'	H-4/4'	H-9/9'	H-7/7'
pH* 7.0					
δ	8.52	7.47	7.39	4.02	3.91
Δδ (**MSS**)	0.15	0.17	0.27	0.00	0.11
Complex c [c]	H-8m	H-6m	H-4m	H-9m/H-9'm	H-7m
pH* 7.0					
δ	8.09	7.39	7.27	3.61 / 3.39	3.82
Δδ (**m-MSS**)	-0.36	0.02	0.08	0.21 / - 0.01	-0.06
Complex d [e]	H-8/8'	H-6/6'	H-4/4'	H-9/9'	H-7/7'
δ	8.52	7.47	7.40	4.01	3.91
Δδ (**MSS**)	0.15	0.17	0.28	-0.01	0.11

[a] δ values, in ppm, relative to Me4Si, using tert-butyl alcohol (δ_H = 1.2) as an internal reference.
[b] 5 mmol dm^{-3} **MSS** solution; [c] 5: 5 mmol dm^{-3} Al(III) / **MSS** solution; [e] an aqueous solution of the **Al(III)** / **MSS** complex synthesized in DMSO, pH* 4.88.

*2.2. DFT structural characterization of the **Al(III) / MSS** complex*

As mentioned in the previous section, the synthesized complex **d=b** is expected to have a 1 : 1 (metal : ligand) stoichiometry and formula $[Al(MSS)(H_2O)_2]^-$, since one molecule of the Schiff base **MSS**, which is tetradentate, coordinates one octahedral aluminium centre and two molecules of H_2O are coordinated to the remaining apical positions of the aluminium metal centre. To help elucidate the coordination mode of Al^{3+} with **MSS** in solution, the structures of the possible isomers of the complex have been optimized at the DFT level. Four isomers were found, with different relative positions of the methoxy groups. These isomers present different torsional angles of the CC – OCH_3 coordinates, and

result from a balance between electronic effects, such as conjugation or dipole-dipole interactions that stabilize specific conformations, and torsional strain. The results are summarized in Figure 5 and Table 3. The calculations show that conformer I, which has C_2 symmetry, is the most stable form of the **Al(III) / MSS** complex. The shortest Al–N_5 (1.986 Å) and Al–O_3 (1.828 Å) bonds are found for this isomer and, because of its symmetrical features, they are equivalent to Al–N_6 and Al–O_4, respectively. The second most stable form is conformer II, with a ΔG^o of 1.3 kJ mol^{-1} relative to conformer I. This energy difference between conformer I and conformer II results in approximate populations of 59% and 35%, respectively (conformers III and IV have populations of 5.89% and 0.16%, respectively). Since only one 1 : 1 (symmetrical) complex is observed in the NMR spectra, we propose that this complex is conformer I. Table 4 includes a list of selected structural parameters for this structure.

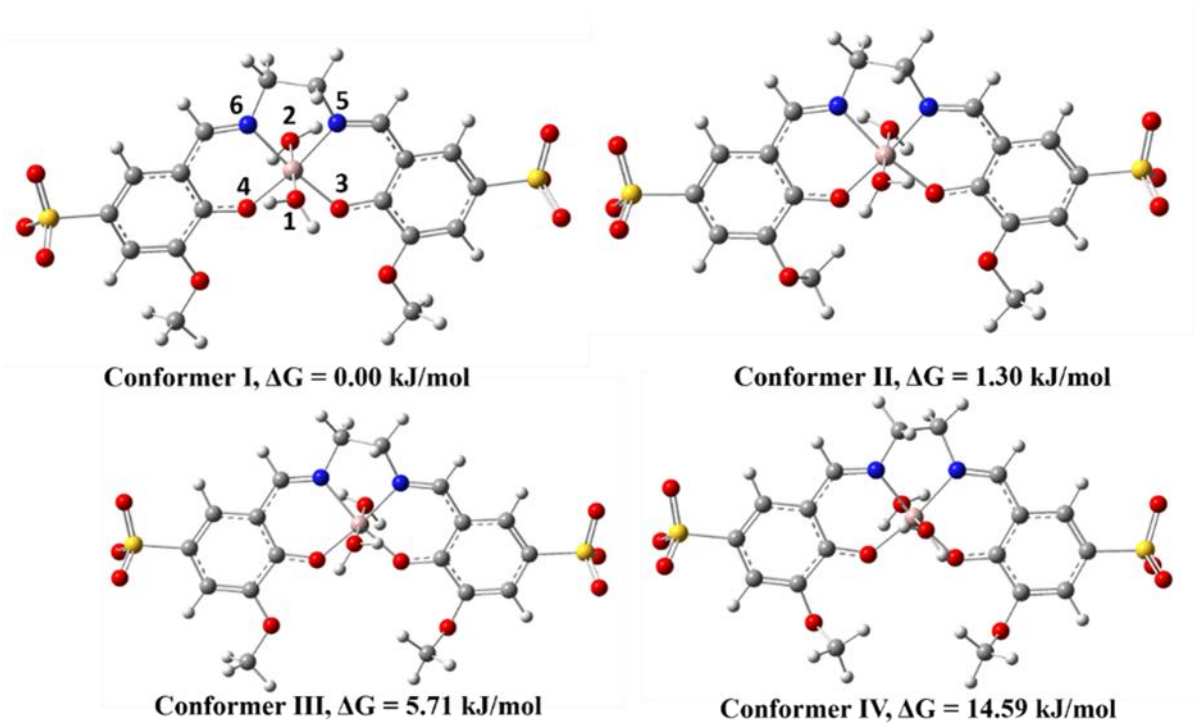

Figure 5. DFT(B3LYP)/6–311++G(d,p) optimized geometries of the most stable conformers of **Al(III) / MSS** considering the bulk effects of water solvent.

Table 3. DFT(B3LYP)/6–311++G(d,p) calculated relative electronic energies (ΔE_{el}) (kJ mol^{-1}), zero-point-corrected electronic energies (ΔE_{Total}), Gibbs energies at 298.15 K (ΔG_{298K}), and equilibrium populations (%) estimated from the relative Gibbs energies (P_{298}), of the synthesized complex **Al(III) / MSS**, considering the bulk effects of water solvent.

Structure	Conformer I	Conformer II	Conformer III	Conformer IV
Symmetry	C_2	C_1	C_1	C_1
ΔE_{el} (kJ/mol)	0.0	6.9	6.9	17.1
$\Delta(E_{total})$ (kJ/mol)	0.0	7.3	7.4	15.5
ΔG^o_{298k}	0.0	1.3	5.7	14.6

P_{298} (%)	59.0	35.0	5.9	0.2

Table 4. Selected bond lengths (Å), bond angles (◦) and dihedral angles (◦) of **Al(III) / MSS** calculated at the DFT(B3LYP)/6–311++G(d,p) level in aqueous solution (IEF-PCM model).

Bond lengths (Å)		Bond Angles (◦)		Dihedral Angles (◦)	
Al-O_1	2.03	O_1-Al-O_2	180	O_1-Al-O_2-O_3	132
Al-O_2	2.03	O_1-Al-N_5	90	O_1-Al-O_3-N_5	110
Al-O_3	1.83	O_1-Al-O_3	87	O_3-Al-N_6-O_2	110
Al-O_4	1.83	O_3-Al-O_4	96	O_3-Al-N_5-O_4	163
Al-N_5	1.98	N_5-Al-N_6	82	N_6-Al-O_3-O_4	162
Al-N_6	1.98	N_5-Al-O_3	91	N_6-Al-O_3-O_1	70

*2.3. SEM and EDX analysis of **Al(III) / MSS***

The morphology of the synthesized **Al(III) / MSS** complex was established by scanning electron microscopy (SEM) as shown in Figure 6 (a). Energy-dispersive X-ray (EDX) was carried out as shown in Figure 7, which demonstrated that the sample contains the elements Al (aluminum), C (carbon), N (nitrogen), O (oxygen), S (sulfur), and Na (sodium) in amounts in accordance with the proposed structure for the **Al(III) / MSS** complex, with the atomic ratios 2.57, 48.95, 5.16, 32.51, 5.73, and 5.08 %, respectively. The atomic percentages are summarized in Table 5. Furthermore, investigation of EDX-mapping indicates a uniform distribution of these elements in the sample (Figure 6 (b)), which confirmed that the **Al(III) / MSS** complex was successfully synthesized without other impurities being identified, in complete agreement with the NMR (Section 2.1), and DFT findings (Section 2.2).

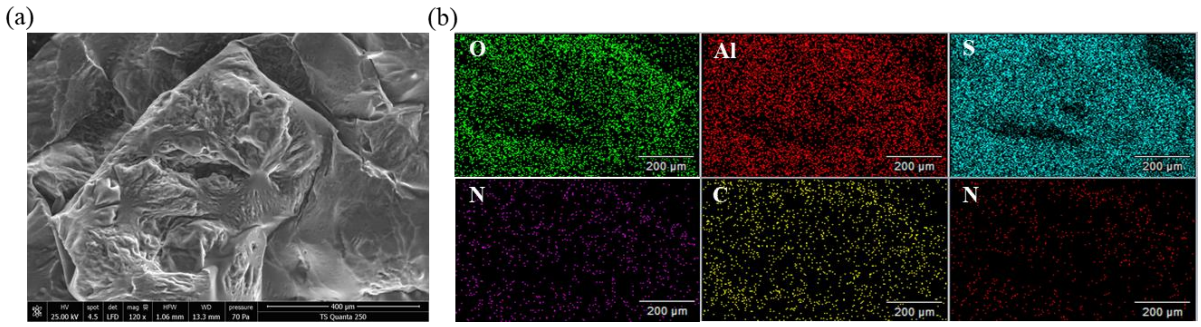

Fig. 6. SEM image (a), EDX mapping images (b) of **Al(III) / MSS** (Scale bar=200 µm).

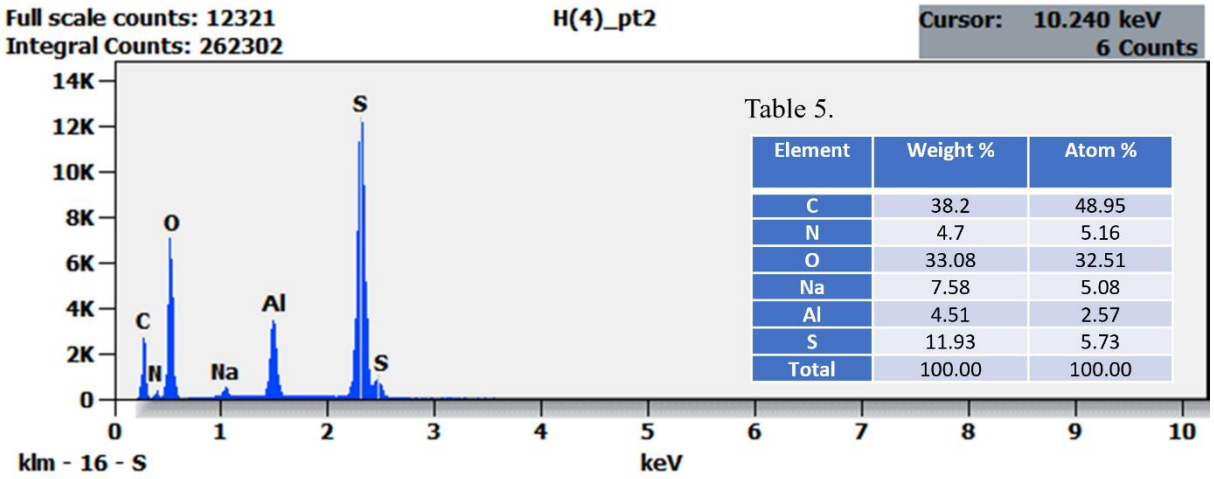

Table 5.

Element	Weight %	Atom %
C	38.2	48.95
N	4.7	5.16
O	33.08	32.51
Na	7.58	5.08
Al	4.51	2.57
S	11.93	5.73
Total	100.00	100.00

Fig. 7. EDX results of **Al(III) / MSS**.

*2.4 ATR–FTIR and Raman studies on the **Al(III) / MSS** system*

Figure 8 displays the ATR–FTIR spectra of **MSS** and its Al(III) complex spanning the 1800 to 400 cm^{-1} region. This analysis aims to provide additional comprehensive insights into the structure of the synthesized complex **Al(III) / MSS** (middle) by comparing it with the spectra of solid **MSS** (top) and solid aluminum nitrate nonahydrate (bottom).

The middle spectrum reveals clear indications of complexation between Al(III) and the ligand **MSS**, evident by the presence of new bands at 1662, 1556, 1329, 1314, 810, 645, 491, and 429 cm^{-1}. Moreover, the absence of the band at 1526 cm^{-1} and the increase in the intensity of the band at 616 cm^{-1} are also indications of complexation. Additionally, bands at 1648 cm^{-1}, and 1601 cm^{-1} are shifted relative to the ligand bands (1634 cm^{-1} and 1608 cm^{-1}, respectively). All these modifications clearly reveal the formation of a complex between Al(III) and **MSS**.

The spectra of the ligand and complex within the 4000–2500 cm^{-1} region (Figure S8) are dominated by broad and strong bands arising from the symmetrical and anti-symmetrical stretching vibrations of the NH, CH_2 and CH_3 groups of **MSS**, along with coordinated H_2O molecules in the complex, as well as hygroscopic H_2O in the samples. Additionally, the stretching vibrations of the sp^2 C–H aromatic bonds are observed close to 3000 cm^{-1}.

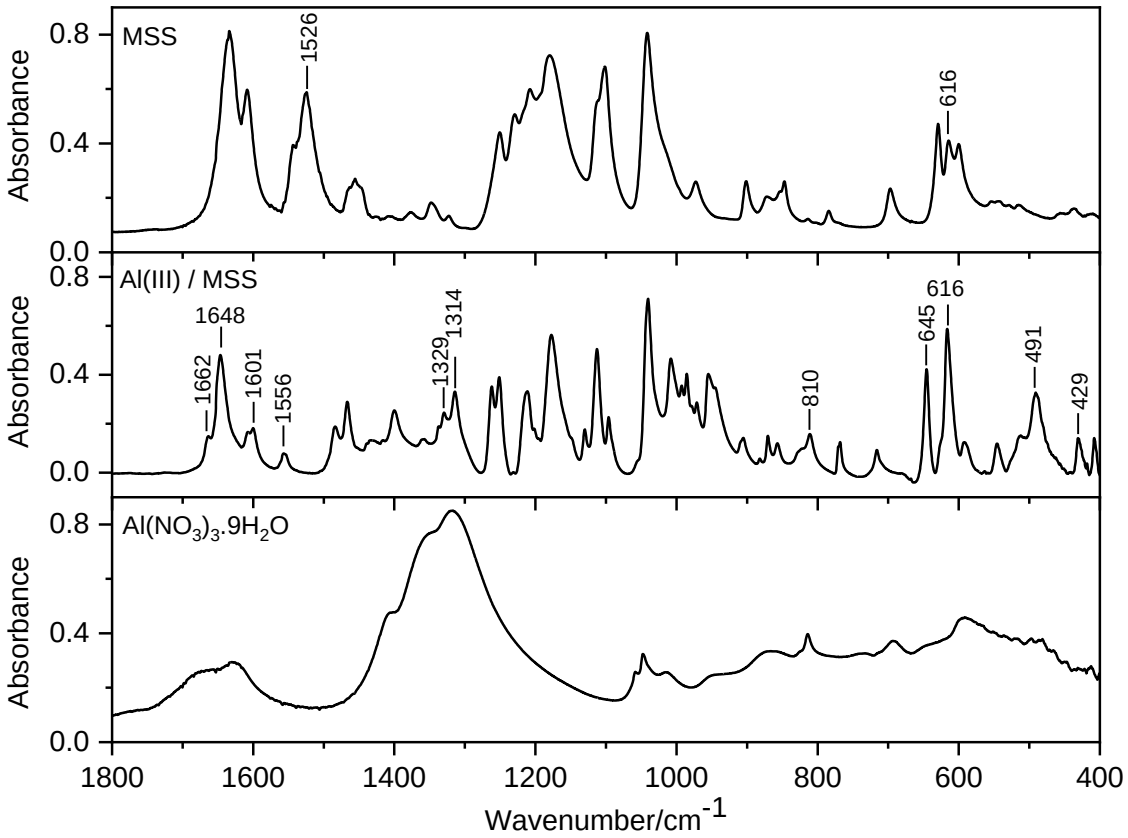

Figure 8. ATR–FTIR spectra (1800 – 400 cm^{-1}) of solid $Al(NO_3)_3.9H_2O$ (bottom), solid **Al(III) / MSS** (middle), and solid **MSS** (top).

To thoroughly analyze the FTIR-ATR spectra of the samples, the vibrational frequencies and intensities were computed using DFT at the B3LYP/6-311++G(d,p) theory level for both the **MSS** ligand and the optimized structure of the complex **Al(III) / MSS** (conformer I). The computed spectra for the ligand and complex are displayed in Figure 9 in comparison with the experimental spectra (the full spectra can be seen in Figure S8).

Although direct information on the solid-state conformation of the ligand **MSS** is not provided by the DFT calculations, by calculating the vibrational spectrum for each of the conformers of **MSS** and comparing them with the experimental spectrum, one can draw conclusions on the most probable conformation of the ligand in the solid state. This analysis was done for the nine conformers presented in Figures 1 and S3 and we could conclude that conformer IV-a-NH (Figure 1) allowed accurate reproduction of the main bands of the experimental spectrum of the solid **MSS**, particularly in the spectral region above 1200 cm^{-1}. This observation suggests that the Schiff base **MSS** predominantly adopts the keto form in the solid state. This result is expected taking into account the greater stability predicted for the keto-enamine form in both water and DMSO solutions, and is likely related with the establishment of stabilizing intermolecular interactions in the solid, as found for related compounds [45].

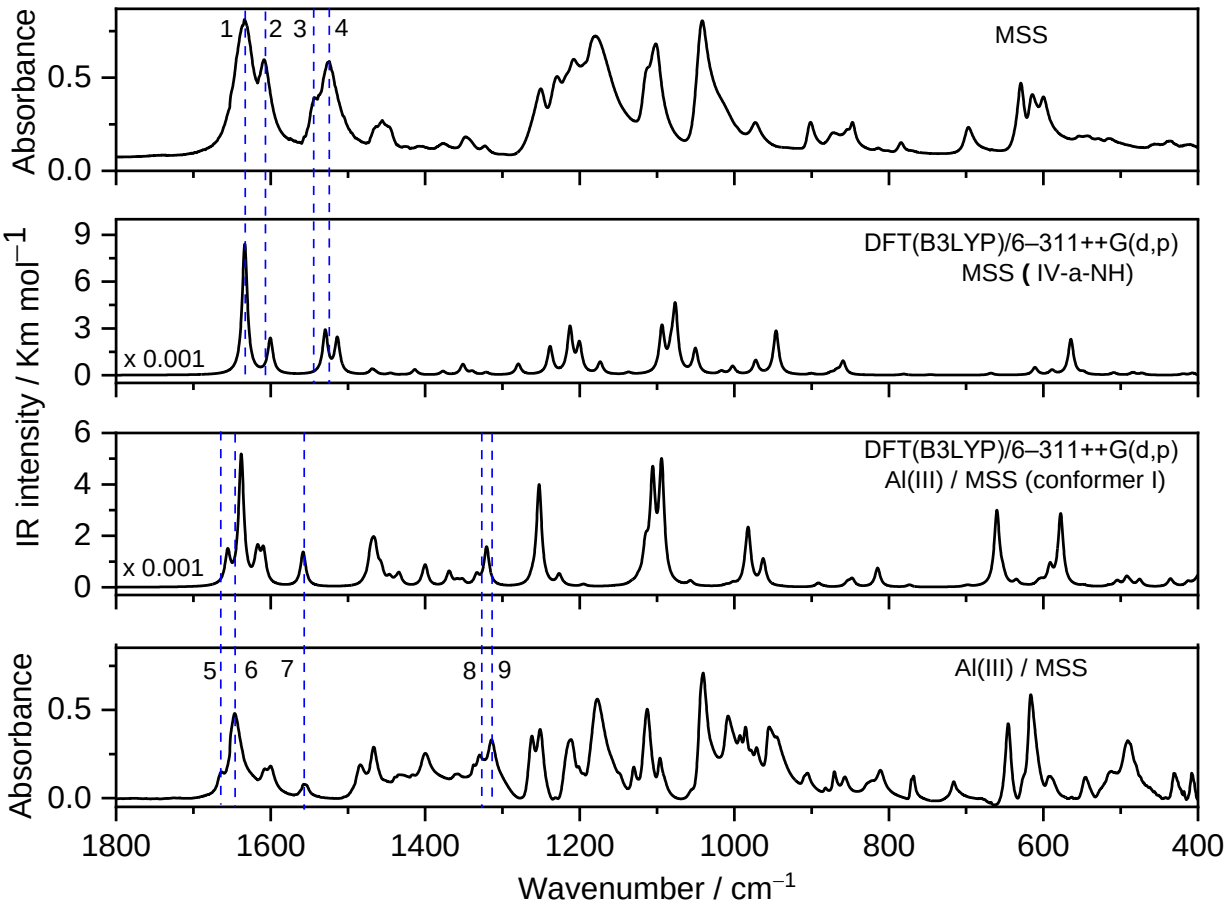

Figure 9. DFT(B3LYP)/6–311++G(d,p) calculated infrared spectra of **MSS** (middle top) and **Al(III) / MSS** (middle bottom), in comparison with the corresponding experimental spectra. Note the multiplication factor 0.001 for the theoretical curves.

Within the spectral region of 1700–1500 cm^{-1}, the experimental spectrum exhibits four bands at 1634 (band 1), 1608 (band 2), 1542 (band 3), and 1526 (band 4) cm^{-1}, which were predicted at 1633, 1600, 1529, and 1514 cm^{-1}, respectively, at the B3LYP/6-311++G(d,p) level of theory. DFT calculations indicate that the band at 1634 cm^{-1} (predicted at 1633 cm^{-1}) is mainly due to the νCN stretching mode, while the band observed at 1608 cm^{-1} (predicted at 1600 cm^{-1}) arises from the stretching of the ring CC bonds and the C=O groups. The lower frequency bands (observed at 1542 and 1526 cm^{-1}) are due to the ring νCC stretching and νC=O stretching modes combined with νC–OCH_3 and in-plane bending of the NH groups, respectively. The low frequencies observed for the stretching mode of the C=O groups are reasoned by the fact that these groups are involved in intramolecular H-bonds.

The most significant differences identified in the experimental infrared spectrum of the solid **Al(III) / MSS** sample, compared to the experimental spectrum of **MSS** (Figures 8 and 9), concern the bands at 1662 (band 5), 1648 (band 6), 1556 (band 7), 1329 (band 8) and 1314 (band 9) cm^{-1}. Accordingly, these bands are predicted for the complex at 1656, 1639, 1559, 1334 and 1321 cm^{-1}, respectively, and are absent from both the theoretical and experimental spectra of **MSS**. The bands predicted at 1656 and 1639

cm^{-1} are due to the νCN stretching modes, while the band predicted at 1559 cm^{-1} is due to the ν$C–OCH_3$ stretching mode, combined with ring νCC stretching. The bands predicted at 1334 and 1321 cm^{-1} involve contributions from the νC=O stretching mode combined with ring CC in-plane bending. Additionally, the experimental intense bands with maxima at 1260 and 1250 cm^{-1} are most likely related with the bands predicted at 1253 and 1252 cm^{-1}, respectively, which have significant contributions from ring in-plane bending vibrations combined with ν$C–OCH_3$. These findings are particularly significant since they confirm the involvement of the C=O and C-N groups in metal coordination, which is completely consistent with the NMR and DFT findings. Given the weakening of the C=O bond caused by ligand-metal electron donation, it is expected that the νC=O stretching mode will move to a lower wavelength during complexation.

The bands below 1200 cm^{-1} in ligand and complex spectra were challenging to assign due to intermolecular interactions, including H-bonding, which involve the polar groups of the ligand and, possibly, hygroscopic water. The bands observed at 1100, 1040 and 900 cm^{-1} for **MSS** were influenced by the complexation and found at 1113, 1040, 945 cm^{-1} in **Al(III) / MSS**. Based on the computed frequencies, these bands are attributed to the anti-symmetrical and symmetrical stretching vibrational modes of the sulfonate group combined with ring vibrations and νOC7. Additionally, the new observable vibrational bands found at 810, 645, 491 and 429 cm^{-1}, predicted at 815, 661, 476 and 436 cm^{-1} in **Al(III) / MSS**, are assigned to skeletal vibrations (that is, vibrations involving the whole molecule) and to vibrations involving the AlO_2N_2 metal center and the coordinated water molecules.

The Raman spectra (1800 – 400 cm^{-1}) of the solid **MSS** (top) and solid **Al(III) / MSS** (middle bottom) are shown in Figure 10, and they are compared with the spectra calculated for **MSS** (middle top) and **Al(III) / MSS** (bottom) using DFT(B3LYP)/6–311++G(d,p) (the full spectra are provided in Figure S9).

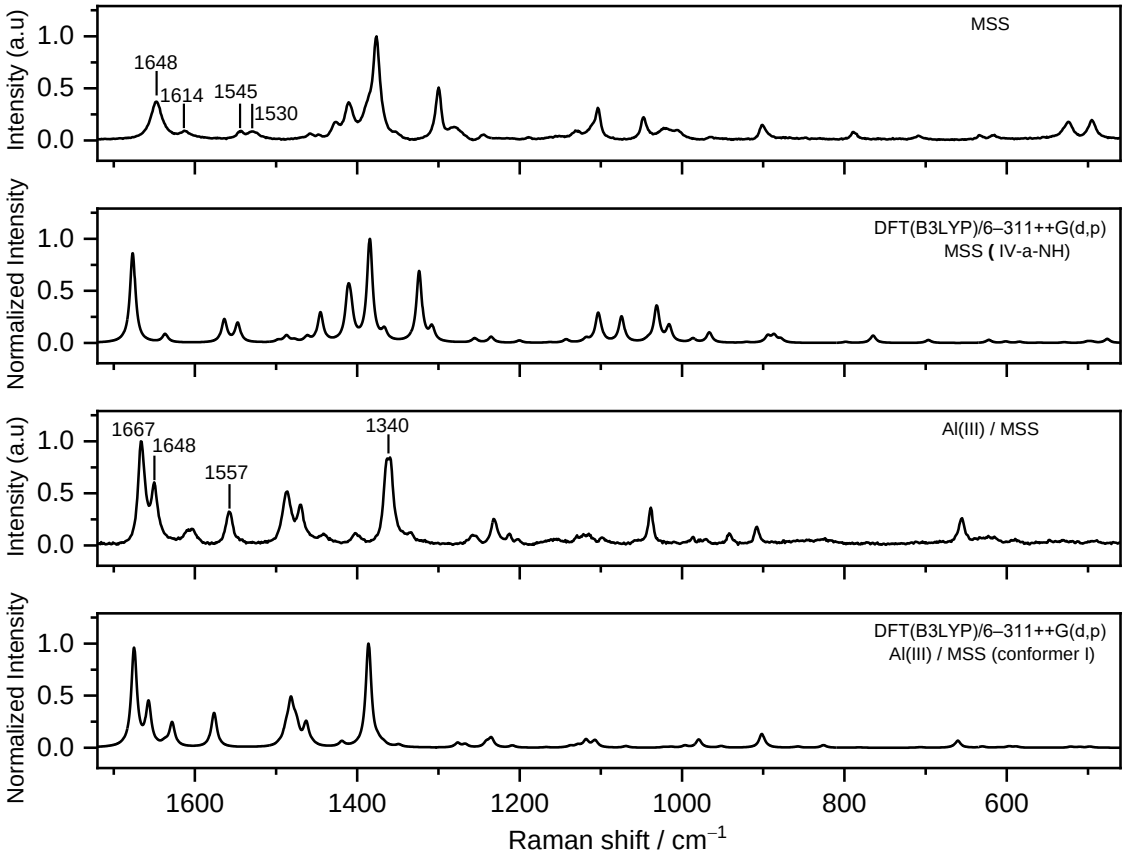

Figure 10. Raman spectra of solid **MSS** (top) and solid **Al(III) / MSS** (middle bottom), compared with the DFT(B3LYP)/6–311++G(d,p) calculated spectra of **MSS** (middle top) and **Al(III) / MSS** (bottom). Baseline due to photoluminescence has been subtracted from the experimental spectra.

The computed spectra reproduce the experimental Raman spectra very well, as they did for the IR spectra. The successful reproduction of the observed Raman intensities by the calculations must be highlighted, since in general Raman intensities are less well predicted theoretically than the IR ones. The vibrational spectrum calculated for IV-a-NH accurately reproduces the main bands of the actual spectrum of the solid **MSS**, particularly in the spectral range above 1200 cm^{-1}. This reinforces the conclusion that the Schiff base, **MSS**, is mostly found in the solid state in the keto form. Four bands were found in the experimental spectrum of **MSS** in the 1700–1200 cm^{-1} spectral region at 1648, 1614, 1545 and 1530 cm^{-1}. At the B3LYP/6-311++G(d,p) level of theory, these bands were predicted at 1677, 1637, 1564 and 1547 cm^{-1}, respectively. The assignment of these bands with a high degree of confidence was made possible by the good agreement between the calculated and measured frequencies. The calculations indicate that the ν*C*N stretching mode is primarily responsible for the band observed at 1648 cm^{-1} in the experimental spectrum (predicted at 1677 cm^{-1}), while the combination of C=O group stretching and the ring ν*C*C stretching is responsible for the band observed at 1614 cm^{-1} (predicted at 1637 cm^{-1}). The lower

frequency bands (1545 and 1530 cm^{-1}) are attributable to the νC–OCH_3 and νC=O stretching modes and νC=O mixed with the in-plane bending of the N–H groups, respectively.

Concerning the differences between the experimental Raman spectra of the solid **Al(III) / MSS** and **MSS** samples (Figure 10), the most significant changes involve the bands observed at 1667, 1648, 1557 and 1340 cm^{-1} in the spectrum of the solid **Al(III) / MSS** sample. Accordingly, these bands are predicted for the complex at 1675, 1657, 1576, and 1349 cm^{-1}, and correspond to the most significant differences between the theoretical spectra of the complex and ligand. The bands predicted at 1675 and 1657 cm^{-1} are due to the νCN stretching mode. These bands are shifted to higher wavenumber (νCN of **MSS** is observed at 1648 cm^{-1}), which shows that the nitrogen of azomethine group is coordinated to the aluminum ion. The band predicted at 1576 cm^{-1} is due to the νC–OCH_3 stretching modes, combined with ring νCC stretching and the band predicted at 1349 cm^{-1} involves contributions from the νC=O stretching mode combined with ring in-plane bending. Finally, the δAlOO'NN' + δH_2O vibrational modes of the complex are observed at 655 cm^{-1} (predicted at 668 cm^{-1}). These results prove particularly valuable since they confirm the participation of the C=O and C-N groups in the coordination to the metal, in complete agreement with the NMR, DFT, and ATR–FTIR findings.

Table 6. Assignment of selected ATR–FTIR and Raman bands of **MSS** and **Al(III) / MSS**.[a]

Experimental		**Calculated**				
IR (Neat solid) ν	**R (Neat solid) ν**	**$ν^{IR}$ (scaled)**	**$ν^{R}$ (unscaled)**	**I^{IR}**	**I^{R}**	**Approximate Assignments[b]**
MSS						
n.obs.	1648	1640	1677	0.000	0.944	ν CN s
1634	n.obs.	1633	1670	2478.9	0.000	ν CN as
n.obs.	1614	1601	1637	0.000	0.086	ν C=O + ν CC ph
1608	n.obs.	1600	1636	667.2	0.000	ν C=O + ν CC ph
n.obs.	1545	1529	1564	0.000	0.233	ν C=O + ν C–OCH_3 + ν CC ph
1542	n.obs.	1529	1564	816.7	0.000	ν C=O + ν C–OCH_3 + ν CC ph
1526	n.obs.	1514	1548	672.5	0.000	ν C=O + ν CC ph + δ NH
n.obs.	1530	1513	1547	0.000	0.194	ν C=O + ν CC ph + δ NH
n.obs.	1377	1354	1385	0.000	1.000	ν CC ph
n.obs.	1300	1295	1324	0.000	0.684	tw CH_2
1100	n.obs.	1094	1118	855.2	0.000	ν SO as
n.obs.	1103	1079	1104	0.000	0.241	δ ph
1040	n.obs.	1076	1101	1220.9	0.000	ν SO as
n.obs.	1046	1051	1074	0.000	0.235	ν OC7 + δ ph

900	n.obs.	946	967	833.0	0.000	ν SO s + δ ph
n.obs.	964	945	966	0.000	0.091	ν SO s + ν OC7 + δ ph
Al(III) / MSS						
1662	1667	1656	1675	361.8	1.000	ν CN s
1648	1648	1639	1657	1479.6	0.428	ν CN as
1601	1607	1610	1628	101.3	0.127	ν CC ph+ sci H_2O
1556	1557	1559	1576	383.8	0.274	ν C–OCH_3 + ν CC ph
1329	1340	1334	1349	117.7	0.021	ν C=O s + δ ph
1314	n.obs.	1321	1336	443.3	0.000	ν C=O as + δ ph
1260	n.obs.	1253	1267	1030	0.021	ν C–OCH_3 + δ ph
1250	1257	1252	1267	131.0	0.007	ν C–OCH_3 + δ ph
1113	n.obs.	1106	1119	958.2	0.024	ν SO as + δ ph
1040	n.obs.	1094	1107	1191.4	0.013	ν SO as
945	n.obs.	963	974	298.4	0.000	ν SO s + ν OC7
810	n.obs.	815	824	208.6	0.000	δ skeletal
645	655	661	668	853.5	0.001	δ AlOO'NN' + δ H_2O
616	n.obs.	653	660	90.4	0.056	δ skeletal + δ AlOO'NN' + δ H_2O
491	n.obs.	476	481	80.0	0.000	δ AlOO'NN' + γ H_2O
429	n.obs.	436	441	88.8	0.007	τ AlOO'NN' + γ H_2O

[a] Frequencies in cm^{-1}; calculated infrared frequencies were scaled by 0.978 (**MSS**) and 0.989 (**Al(III) / MSS** complex); calculated Raman intensities of **MSS** and **Al(III) / MSS** were normalized to the bands at 1385 cm^{-1} and 1675 cm^{-1} respectively; calculated IR intensities in km mol^{-1}; n.obs, not observed; [b] ν, stretching; δ, in-plane bending; γ, out-of-plane rocking; tw, twisting; sci., scissoring; τ, torsion; s., symmetric; as., anti-symmetric; skeletal refers to modes distributed all along the molecule.

*2.5. Thermal analysis on the **Al(III) / MSS** system*

To verify the presence of coordinated water molecules in the complex, the thermal properties of the Schiff base **MSS** and its Al(III) complex were determined using DSC (Figure 11). For **MSS**, the initial peak at 67.44°C reveals the presence of weakly adsorbed water, (ΔH = 19.67 J/g). On the other hand, the **Al(III)/MSS** complex has an endothermic peak at 101.14°C and a higher enthalpy (ΔH = 208.48 J/g), which indicates that the water molecules are coordinated. This transition is similar to the thermal dehydration seen in metal-Schiff base complexes, which was reported by Rajendra et *al*. [55]. Additionally, complexation with Al(III) increased thermal stability, raising the complex's decomposition temperature to 281.48°C from 239.20°C for **MSS**. In the complex, the enthalpy for the second peak is only 13.012 J/g, while it is 380.34 J/g for **MSS**. This shows that the Schiff base breaks down in a single step in the free ligand but in a series of steps in the complex. These results also demonstrate the **Al(III)/MSS** complex's formation and coordination-induced structural changes.

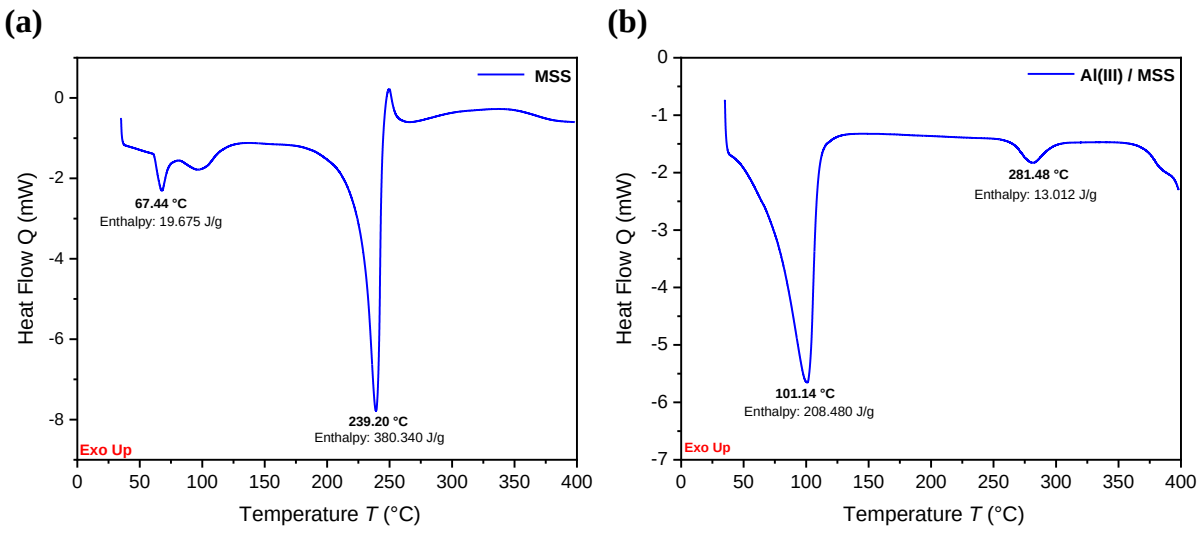

Figure 11. DSC heating curves for (a) **MSS** and (b) **Al(III) / MSS**

Conclusions

In this work, a new water soluble di-Schiff base *N,N'*-bis(3-methoxy-5-sulfonatosalicylidene)-1,2-ethylenediamine disodium salt (**MSS**) was successfully synthesized from sodium 3-methoxy-salicylaldehyde-5-sulfonate (**5-S-3-OMe**) and 1,2-ethylenediamine using both conventional heating and microwave-assisted conditions. Detailed characterization of **MSS** was carried out using a variety of techniques, including ^{1}H and ^{13}C NMR, HRMS, ATR-FTIR and Raman spectroscopies, as well as DFT calculations.

Subsequently, **MSS** was used in complexation studies in aqueous solution and to synthesize a novel Al(III) complex in non-aqueous media (DMSO). The enol-imine (O-H···N) / keto-enamine (O···H-N) relative stability of **MSS** in solution and solid state, and the influence of the intra- and intermolecular interactions in this balance were studied in detail.

Based on DFT results, the enol-imino form is anticipated to be the most stable tautomer in gas phase. On the other hand, the keto-enamine form was identified as the dominant tautomer in water and DMSO solvents and in the solid state (as indicated by both spectroscopic and theoretical studies). Whereas the ligand **MSS** was found to be stable in organic solvents (DMSO, DMF), in aqueous solution its ^{1}H NMR spectra are quite complex, revealing the formation of hydrolytic species, identified as the aldehyde (**5-S-3-OMe**) and ethylenediamine precursors, and the mono-Schiff base (**m-MSS**). In acidic solutions (pH 4), the degradation is complete in a period of 20 minutes. However, at higher pH values (pH 7), the NMR studies demonstrated that when the concentration of **MSS** is in the order of 5 mmol dm^{-3}, about 100

times higher than that used for UV–vis spectroscopy, the degradation is far from complete. The stability of **MSS** towards hydrolysis was compared with that of **SS** (its non-substituted analogue) and it was found that differences in the tautomeric equilibria of the two Schiff bases, along with different susceptibilities of their structures towards nucleophilic attack by water (analyzed on the basis of the charges on the imine carbons), resulted in the observed slower hydrolysis of **SS**.

By using multinuclear (^{1}H and ^{27}Al) NMR spectroscopy, combined with theoretical calculations, a detailed structural characterization of the complexation of Al^{3+} with the ligand **MSS** in aqueous solution has been done. The results revealed the formation of a stable Al(III) complex with **MSS** and additional complexes with its degradation products in the pH range 4–7. The only complex detected at pH 4 is the 1:2 species $[Al(5\text{-}S\text{-}3\text{-}OMe)_2(H_2O)_2]^-$. Moreover, at pH 7, both the 1:2 $[Al(m\text{-}MSS)_2(H_2O)_2]^-$ and the 1:1 $[Al(MSS)(H_2O)_2]^-$ complexes were formed. A comparison of the ^{1}H NMR spectra of the 1:1 Al(III):MSS complex with the synthesized one strongly suggests that they are the same species. DFT calculations indicate that the synthesized **Al(III) / MSS** complex adopts an octahedral geometry, in which one tetradentate Schiff base **MSS** ligand coordinates to a central aluminum atom, with two H_2O molecules occupying the remaining apical positions. The accurate reproduction of the experimental infrared and Raman spectra of the synthesized **Al(III) / MSS** complex based on the theoretical calculations, provides further support for the DFT proposed structure. Preliminary results using UV–vis absorption and reflectance spectroscopy have indicated that the compound is a wide band gap semiconductor and might have potential applications in photocatalysis. Future studies are planned to investigate this.

Experimental and computational methods

Materials. The research chemicals, salicylaldehyde, *ortho*-vanillin (3-methoxysalicaldehyde), aniline, 1,2-ethylenediamine, concentrated sulfuric acid, glacial acetic acid, anhydrous sodium carbonate, and aluminum nitrate nonahydrate ($Al(NO_3)_3 \cdot 9H_2O$) used in this study were purchased from commercial suppliers and used as provided. Solvents (water, Millipore Milli-Q water, ethanol, methanol, dimethylformamide (DMF), dimethylsulfoxide (DMSO), toluene, and diethyl ether) were used as supplied or distilled.

Thin-layer chromatography (TLC) analyses were conducted on precoated silica gel plates. For ^{1}H and ^{13}C nuclear magnetic resonance (NMR) studies, the solutions were prepared in hexadeuterated dimethylsulfoxide DMSO-d_6 (99.8% D) or deuterium oxide D_2O (99.9% D) and the pH was adjusted by addition of DCl and NaOD (Aldrich).

Physical measurements. The infrared (attenuated total reflectance-ATR) spectra were acquired at room temperature using a Thermoscientific Fourier Transform Infrared Spectrometer—Nicolet iS5. An iD7

ATR Accessory was used to record the spectra with a resolution of 2 cm^{-1}. The Raman spectra were acquired with a ~4 cm^{-1} spectral resolution using a LabRAM HR Evolution Raman microscope (Horiba Scientific) with a 600 gr/mm grating. The excitation was provided by a He-Ne laser (λ = 633 nm) focused on the sample to a ~1 mm spot using a 100× objective. The applied laser power of ~0.2 mw at the sample resulted in no detectable heating or degradation. The collection time was 10 s with 100 accumulations being averaged to generate the final spectra.

The ^{1}H NMR (400 MHz) and ^{13}C NMR (100 MHz) spectra were obtained on a Brucker Avance III-400 NMR spectrometer and the ^{27}Al NMR (156.4 MHz) spectra were obtained on a Brucker Avance III-600 NMR spectrometer. Chemical shifts are expressed in parts per million (ppm) relative to internal tetramethylsilane (TMS). The methyl signal of *tert*-butyl alcohol was used as an internal reference for ^{1}H (δ 1.2) and ^{13}C (δ 31.2) relative to TMS and a solution of $Al(NO_3)_3$ acidified at pH 2.0, $[Al(H_2O)_6]^{3+}$, (δ 0), as an external reference for the ^{27}Al NMR spectra. The ^{13}C spectra were acquired using proton decoupling techniques (Waltz-16) which take use of the nuclear Overhauser effect. Consequently, signal intensities for ^{13}C spectra are not quantitative.

The high-resolution mass spectrum (HRMS) was obtained on a Thermo Orbitrap Q-Exactive Focus spectrometer with electrospray ionization (ESI). Melting points have been determined in open glass capillaries.

Scanning Electron Microscopy (SEM, Q250) with 15 KV of accelerating voltage and energy-dispersive analysis with X-rays (EDX) Jeol JEM 2100 HR coupled with CCD (Charge Coupled Device) Gatan Orius SC200D with an acceleration voltage 200 kV from the source (LaB6) were used to characterize and to investigate the morphology of the synthesized complex.

The UV–vis absorption spectra were measured on a Shimadzu 2600 UV–vis spectrophotometer. All samples were kept in the absence of light when not in use for measurements. The concentration of the samples utilized in the UV–vis studies were in the range of 1.0×10^{-5} mol dm^{-3} to 1.0×10^{-4} mol dm^{-3}.

Differential Scanning Calorimetry (DSC) measurements were recorded on raw powders with TA DSC 25 instrument under nitrogen atmosphere, in the temperature range between 0 °C to 400 °C with heating rate of 10 °C.min^{-1}. The TRIOS software version v5.0.0.44608 was utilized to analyze the DSC thermogram plots for the determination of enthalpy changes and phase transformation temperatures.

Computational details. The new di-Schiff base synthesized in this study, **MSS**, is an acyclic structure with a significant number of rotational degrees of freedom and, therefore, can adopt many conformations. In order to identify the most stable conformations of this ligand, we began by conducting a conformational search at the molecular mechanics (MM) level of theory, in which 1000 conformers were generated using

the MMFF94 force field [56] implemented in the MarvinSketch program [57]. Of these conformers, the 150 lowest energy structures, corresponding to those within a limit of 13.3 kJ mol^{-1} above the lowest energy form, were optimized at the density functional theory level (DFT/B3LYP) [58–60] using Gaussian 16 [61], with the extended split-valence triple-ζ plus polarization 6-311++G(d,p) basis set [62–64]. The calculations were undertaken in gas phase and in two solvents, the bulk solvent effects of water and dimethyl sulfoxide being simulated using the integral equation formalism variant of the polarized continuum model (IEF-PCM), within the self-consistent reaction field (SCRF) theoretical framework [65,66] (note that this model does not account for specific interactions with the solvent molecules). The input geometries for the *N,N'*-bis(5-sulfonatosalicylidene)-1,2-ethylenediamine disodium salt (Schiff base **SS**) tautomers were built based on the **MSS** tautomers (by removing the methoxy groups) and were optimized in water. The geometries of the Al^{3+} complexes were optimized using the same functional and basis sets. Whenever applicable, the geometry optimization was completed with the imposition of symmetry. The vibrational frequencies of all optimized structures were evaluated to ensure that they are true minima. The theoretical IR spectra of the lowest energy conformers of the free ligand **MSS** and **Al(III) / MSS** complex were obtained after scaling the calculated harmonic vibrational wavenumbers by 0.978 and 0.989, respectively, mainly to account for the effects of basis set limitations, neglect of part of electron correlation and anharmonicity (the first value is our standard scaling factor for the combination of method and basis set used in the optimization of small organic molecules [67–69], and the second scaling factor was obtained by a linear regression fit between selected calculated and experimental frequencies for the complex). The NMR calculated data for the optimized geometries were obtained using the Gauge-Independent Atomic Orbital (GIAO) approach [70–74] at the B3LYP/6-311++G(d,p) level of theory, considering the bulk solvent effects of water. The calculated ^{1}H GIAO absolute shieldings (σ; ppm) were converted into chemical shifts (δ values; ppm) by subtracting them from the TMS GIAO calculated absolute shielding. (31.98 ppm for ^{1}H).

Synthesis of Schiff bases and complex. The procedures for the syntheses of *N,N'*-bis(5-sulfonatosalicylidene)-1,2-ethylenediamine disodium salt (Schiff base **SS**) and sodium 3-methoxy-salicylaldehyde-5-sulfonate (**5-S-3-OMe**) are described in the Supplementary Material.

*Synthesis of the Schiff base **MSS** by conventional heating method:* To a suspension of **5-S-3-OMe** (305 mg, 1.2 mmol) in methanol (11 mL), a solution of 1,2-ethylenediamine (54 mg, 0.9 mmol) in ethanol (1.5 mL) was added dropwise and the reaction mixture was stirred at 80 °C for 2 h. After cooling to room temperature, the precipitate was filtered, washed with cold methanol, and dried to give **MSS** as a yellow solid. Yield: 0.43 g (0.8 mmol, 66%).

*Synthesis of the Schiff base **MSS** under microwave irradiation (MW):* Sodium 3-methoxy-salicylaldehyde-5-sulfonate (**5-S-3-OMe**) (0.2 g, 0.8 mmol) and 1,2-ethylenediamine (22 mg, 0.35 mmol) were mixed thoroughly in a mortar and pestle. Ethanol (1.5 mL) and a few drops of DMSO were added and the reaction mixture was irradiated in a microwave reactor (CEM Microwave Synthesizer Discover 2.0) at 120 ºC for 45 min. After cooling to room temperature, the precipitate was filtered, washed with cold ethanol, and dried under air to give **MSS** as a yellow solid. Yield: 0.37 g (0.7 mmol, 87%). ^{1}H NMR (DMSO-d_6, 400 MHz, Figure S1 (a)): δ (ppm) 13.76 (bs, 2H), 8.64 (s, 2H), 7.29 (d, J = 1.6 Hz, 2H), 7.17 (d, J = 1.4 Hz, 2H), 3.92 (s, 4H), 3.77 (s, 6H). ^{13}C NMR (DMSO-d_6, 100 MHz, Figure S1 (b)) 167.6, 153.7, 147.9, 138.3, 120.8, 116.7, 112.3, 58.0, 56.0. Melting point > 300 °C. HRMS (ESI, Figure S2): Calc. for $C_{18}H_{19}N_2Na_2O_{10}S_2$ $[M+H]^+$ 533.0271; found 533.0267.

*Synthesis of the **Al(III) / MSS** complex:* The ligand **MSS** (266 mg, 0.5 mmol) and $Al(NO_3)_3 \cdot 9H_2O$ (188 mg, 0.5 mmol) were suspended in anhydrous DMSO (2.5 mL), heated to 80 °C and stirred at this temperature until a clear solution was obtained. After cooling to room temperature, the precipitate was filtered and washed with small portions of toluene and dried under vacuum to give the **Al(III) / MSS** complex as a pale-yellow powder. Yield: 154 mg (0.26 mmol, 52%). ^{1}H NMR (D_2O, 400 MHz, Figure S7 (a)): δ (ppm) 8.52 (s, 2H), 7.47 (d, J = 1.8 Hz, 2H), 7.40 (d, J = 2.0 Hz, 2H), 4.01 (s, 4H), 3.91 (s, 6H). ^{13}C NMR (D_2O, 100 MHz, Figure S7 (b)) 168.5, 156.2, 150.6, 130.4, 123.6, 117.5, 112.0, 55.9, 53.7. Melting point > 300 °C.

Supporting Information

Additional references cited within the Supporting Information [75,76].

Data availability

The data supporting this article has been included as part of the Supplementary Information.

Conflicts of interest

There are no conflicts to declare.

Acknowledgements

The authors acknowledge the financial support from the Portuguese "*Fundação para a Ciência e a Tecnologia*" (FCT), through Projects CQC-IMS UIDB/00313/2020 and UIDP/00313/2020 (national funds; DOI: 10.54499/UIDB/00313/2020 and 10.54499/UIDP/00313/2020) and LA/P/0056/2020. L.L.G.J. acknowledges the financial support from FCT (DL 57/2016/CP1370/CT0032, DOI:

10.54499/DL57/2016/CP1370/CT0032). M.I.L.S. acknowledges the financial support from FCT (DL57/2016/CP1370/CT0041, DOI: 10.54499/DL57/2016/CP1370/CT0041). The authors also thank the Laboratory for Advanced Computing at the University of Coimbra for providing computing resources that have contributed to the research results reported within this paper (URL: https://www.uc.pt/lca). The NMR data was collected at the UC-NMR facility (URL: www.nmrccc.uc.pt) which is supported in part by FEDER – European Regional Development Fund through the COMPETE Programme (Operational Programme for Competitiveness) and by national funds through FCT (Grants REEQ/481/QUI/2006, RECI/QEQ-QFI/0168/2012, CENTRO-07-CT62-FEDER-002012, and *Rede Nacional de Ressonância Magnética Nuclear* (RNRMN)).

References

[1] H. Schiff, Mittheilungen aus dem Universitätslaboratorium in Pisa: Eine neue Reihe organischer Basen, Justus Liebigs Ann. Chem., 131 (1864) 118–119. https://doi.org/10.1002/jlac.18641310113.
[2] S. De, A. Jain, P. Barman, Recent Advances in the Catalytic Applications of Chiral Schiff-Base Ligands and Metal Complexes in Asymmetric Organic Transformations, ChemistrySelect, 7 (2022) e202104334. https://doi.org/10.1002/slct.202104334.
[3] P. Giorgio Cozzi, Metal–Salen Schiff base complexes in catalysis: practical aspects, Chem Soc Rev., 33 (2004) 410–421. https://doi.org/10.1039/B307853C.
[4] W. Radecka-Paryzek, V. Patroniak, J. Lisowski, Metal complexes of polyaza and polyoxaaza Schiff base macrocycles, Coord. Chem. Rev., 249 (2005) 2156–2175. https://doi.org/10.1016/j.ccr.2005.02.021.
[5] P.A. Vigato, S. Tamburini, The challenge of cyclic and acyclic schiff bases and related derivatives, Coord. Chem. Rev., 248 (2004) 1717–2128. https://doi.org/10.1016/j.cct.2003.09.003.
[6] S.M. Gomha, H.A. Ahmed, M. Shaban, T.Z. Abolibda, M.S. Khushaim, K.A. Alharbi, Synthesis, Optical Characterizations and Solar Energy Applications of New Schiff Base Materials, Mater., 14 (2021) 3718. https://doi.org/10.3390/ma14133718.
[7] A.L. Berhanu, Gaurav, I. Mohiuddin, A.K. Malik, J.S. Aulakh, V. Kumar, K.-H. Kim, A review of the applications of Schiff bases as optical chemical sensors, TrAC. Trends Anal. Chem., 116 (2019) 74–91. https://doi.org/10.1016/j.trac.2019.04.025.
[8] W. Fang, Z. Cao, Q. Liu, Y. Chu, H. Zhu, W. Zhou, J. Yang, A novel star-shaped Schiff base compound: Synthesis, properties and application in w-LEDs, Results in Optics, 7 (2022) 100228. https://doi.org/10.1016/j.rio.2022.100228.
[9] J. Zhang, L. Xu, W.-Y. Wong, Energy materials based on metal Schiff base complexes, Coord. Chem. Rev., 355 (2018) 180–198. https://doi.org/10.1016/j.ccr.2017.08.007.
[10] P. Sarkar, S. Sutradhar, B.N. Ghosh, Application in Pharmacological Field, in: P. Barman, A. Singh (Eds.), Schiff Base Metal Complexes, 1st ed., Wiley, 2023: pp. 129–147.
[11] A. Erxleben, Transition metal salen complexes in bioinorganic and medicinal chemistry, Inorganica Chim. Acta., 472 (2018) 40–57. https://doi.org/10.1016/j.ica.2017.06.060.
[12] J.C. Pessoa, I. Correia, Salan vs. salen metal complexes in catalysis and medicinal applications: Virtues and pitfalls, Coord. Chem. Rev., 388 (2019) 227–247. https://doi.org/10.1016/j.ccr.2019.02.035.
[13] P. Pfeiffer, E. Breith, E. Lübbe, T. Tsumaki, Tricyclische orthokondensierte Nebenvalenzringe, Justus Liebigs Ann. Chem., 503 (1933) 84–130. https://doi.org/10.1002/jlac.19335030106.
[14] C.S. Novoa-Ramírez, A. Silva-Becerril, F.L. Olivera-Venturo, J.C. García-Ramos, M. Flores-Alamo, L. Ruiz-Azuara, N/N Bridge Type and Substituent Effects on Chemical and Crystallographic Properties of Schiff-Base (Salen/Salphen) Niii Complexes, Crystals, 10 (2020) 616. https://doi.org/10.3390/cryst10070616.
[15] K. Bakalorz, Ł. Przypis, M. M. Tomczyk, M. Książek, R. Grzesik, N. Kuźnik, Unprecedented Water Effect as a Key Element in Salicyl-Glycine Schiff Base Synthesis, Molecules, 25 (2020) 1257. https://doi.org/10.3390/molecules25051257.
[16] K. Matsumoto, B. Saito, T. Katsuki, Asymmetric catalysis of metal complexes with non-planar ONNO ligands: salen, salalen and salan, Chem Commun., 35 (2007) 3619–3627. https://doi.org/10.1039/B701431G.
[17] C. Baleizão, H. Garcia, Chiral Salen Complexes: An Overview to Recoverable and Reusable Homogeneous and Heterogeneous Catalysts, Chem. Rev. 106 (2006) 3987–4043. https://doi.org/10.1021/cr050973n.

[18] J.F. Larrow, E.N. Jacobsen, Asymmetric Processes Catalyzed by Chiral (Salen)Metal Complexes, in: Organometallics in Process Chemistry, Springer, Berlin, Heidelberg, 2004: pp. 123–152.
[19] L. Canali, D.C. Sherrington, Utilisation of homogeneous and supported chiral metal(salen) complexes in asymmetric catalysis, Chem Soc Rev., 28 (1999) 85–93. https://doi.org/10.1039/A806483K.
[20] A. Gualandi, F. Calogero, S. Potenti, P.G. Cozzi, Al(Salen) Metal Complexes in Stereoselective Catalysis, Mol., 24 (2019) 1716. https://doi.org/10.3390/molecules24091716.
[21] C. Boulechfar, H. Ferkous, A. Delimi, A. Djedouani, A. Kahlouche, A. Boublia, A.S. Darwish, T. Lemaoui, R. Verma, Y. Benguerba, Schiff bases and their metal Complexes: A review on the history, synthesis, and applications, Inorg. Chemi. Commun., 150 (2023) 110451. https://doi.org/10.1016/j.inoche.2023.110451.
[22] S. Nagendran, H.W. Roesky, The Chemistry of Aluminum(I), Silicon(II), and Germanium(II), Organomet., 27 (2008) 457–492. https://doi.org/10.1021/om7007869.
[23] D.A. Atwood, M.J. Harvey, Group 13 Compounds Incorporating Salen Ligands, Chem. Rev., 101 (2001) 37–52. https://doi.org/10.1021/cr990008v.
[24] J.-P. Cornard, C. Lapouge, E. André, pH influence on the complexation site of Al(III) with protocatechuic acid. A spectroscopic and theoretical approach, Spectrochim Acta A Mol Biomol Spectrosc., 108 (2013) 280–287. https://doi.org/10.1016/j.saa.2013.02.005.
[25] C. Ni, X. Ma, Z. Yang, H.W. Roesky, Recent Advances in Aluminum Compounds for Catalysis, Eur J Inorg Chem., 2022 (2022) e202100929. https://doi.org/10.1002/ejic.202100929.
[26] M.R. Mason, Aluminum-Based Catalysis, in: Encyclopedia of Inorganic and Bioinorganic Chemistry, John Wiley & Sons, Ltd, 2015: pp. 1–22.
[27] A. K. Asatkar, M. Tripathi, D. Asatkar, Salen and Related Ligands, in: A. Nanda Srivastva (Ed.), Stability and Applications of Coordination Compounds, IntechOpen, 2020.
[28] P. Di Bernardo, P.L. Zanonato, S. Tamburini, P. Tomasin, P.A. Vigato, Complexation behaviour and stability of Schiff bases in aqueous solution. The case of an acyclic diimino(amino) diphenol and its reduced triamine derivative, Dalton Trans., (2006) 4711–4721. https://doi.org/10.1039/b604211b.
[29] C.A. Hawkins, C.G. Bustillos, I. May, R. Copping, M. Nilsson, Water-soluble Schiff base-actinyl complexes and their effect on the solvent extraction of f-elements, Dalton Trans., 45 (2016) 15415–15426. https://doi.org/10.1039/C6DT01357K.
[30] P. Naumov, M. Kochunnoonny, Spectral−Structural Effects of the Keto−Enol−Enolate and Phenol−Phenolate Equilibria of Oxyluciferin, J. Am. Chem. Soc., 132 (2010) 11566–11579. https://doi.org/10.1021/ja102885g.
[31] W. Wang, H.W. Hellinga, L.S. Beese, Structural evidence for the rare tautomer hypothesis of spontaneous mutagenesis, Proc. Natl. Acad. Sci. U.S.A., 108 (2011) 17644–17648. https://doi.org/10.1073/pnas.1114496108.
[32] S.J. Benkovic, K.J. Schray, Mechanisms of hydrolysis of phosphate ester derivatives of phosphoenolpyruvic acid, J. Am. Chem. Soc., 93 (1971) 2522–2529. https://doi.org/10.1021/ja00739a027.
[33] P.J. Taylor, G. Van Der Zwan, L. Antonov, Tautomerism: Introduction, History, and Recent Developments in Experimental and Theoretical Methods, in: L. Antonov (Ed.), Tautomerism, 1st ed., Wiley, 2013: pp. 1–24.
[34] I. Felker, G. Pupo, P. Kraft, B. List, Design and Enantioselective Synthesis of Cashmeran Odorants by Using "Enol Catalysis," Angew Chem Int Ed., 54 (2015) 1960–1964. https://doi.org/10.1002/anie.201409591.
[35] S. Jiang, T.-S. Yan, Y.-C. Han, L.-Q. Cui, X.-S. Xue, C. Zhang, Hypervalent-Iodine-Mediated Formation of Epoxides from Carbon(sp^2)–Carbon(sp^3) Single Bonds, J. Org. Chem., 82 (2017) 11691–11702. https://doi.org/10.1021/acs.joc.7b00883.
[36] J.E. De Vrieze, J.W. Thybaut, M. Saeys, Role of Keto–Enol Tautomerization in the Copper-Catalyzed Hydrogenation of Ketones, ACS Catal., 9 (2019) 3831–3839. https://doi.org/10.1021/acscatal.9b00279.
[37] G. Kaştaş, Ç.A. Kaştaş, B.K. Kırca, C.C. Ersanlı, The effect of the change in substituents' positions on the formation of supramolecular networks and the solvent type/substituent dependence of prototropic behavior in three new o-hydroxy Schiff bases, J. Mol. Struct., 1200 (2020) 127109. https://doi.org/10.1016/j.molstruc.2019.127109.
[38] S.D. Chatziefthimiou, Y.G. Lazarou, E. Hadjoudis, T. Dziembowska, I.M. Mavridis, Keto Forms of Salicylaldehyde Schiff Bases: Structural and Theoretical Aspects, J. Phys. Chem. B, 110 (2006) 23701–23709. https://doi.org/10.1021/jp064110p.
[39] K.J. Berry, F. Moya, K.S. Murray, A.M.B. van den Bergen, B.O. West, Water-soluble Cobalt(II) Complexes of NN'-Substituted Bis(salicyl-aldimine-5-sulphonic Acids). Oxygen-carrying Properties and Conversion into Cobalt(III) Organometallic Compounds, J. Chem. Soc., Dalton Trans., (1982) 109–116. https://doi.org/10.1039/DT9820000109.
[40] A.K. Gupta, A. Kumar, R. Singh, M. Devi, A. Dhir, C.P. Pradeep, Facile Synthesis of an Organic Solid State Near-Infrared-Emitter with Large Stokes Shift via Excited-State Intramolecular Proton Transfer, ACS Omega, 3 (2018) 14341–14348. https://doi.org/10.1021/acsomega.8b02116.
[41] A. Bhattacharyya, S.C. Makhal, S. Kumar Mandal, N. Guchhait, Exploring the hidden potential of a methoxy substituted HBT derivative as an efficient example of coupling of AIE and ESIPT processes and as an energy harvesting platform, New J Chem., 43 (2019) 15087–15096. https://doi.org/10.1039/C9NJ03340H.

[42] M.J. Reimann, D.R. Salmon, J.T. Horton, E.C. Gier, L.R. Jefferies, Water-Soluble Sulfonate Schiff-Base Ligands as Fluorescent Detectors for Metal Ions in Drinking Water and Biological Systems, ACS Omega, 4 (2019) 2874–2882. https://doi.org/10.1021/acsomega.8b02750.
[43] Z. Chen, S. Guieu, N.G. White, F. Lelj, M.J. MacLachlan, The Rich Tautomeric Behavior of Campestarenes, Chem. A Eur J., 22 (2016) 17657–17672. https://doi.org/10.1002/chem.201603231.
[44] L. Antonov, W.M.F. Fabian, D. Nedeltcheva, F.S. Kamounah, Tautomerism of 2-hydroxynaphthaldehyde Schiff bases, J. Chem. Soc., Perkin Trans. 2 (2000) 1173–1179. https://doi.org/10.1039/b000798f.
[45] M. Rocha, D.M. Gil, G.A. Echeverría, O.E. Piro, J.L. Jios, S.E. Ulic, Enol-imino–Keto-enamine Tautomerism in a Diazepine Derivative: How Decisive Are the Intermolecular Interactions in the Equilibrium?, J. Org. Chem. 84 (2019) 11042–11053. https://doi.org/10.1021/acs.joc.9b01533.
[46] M.S.S. Adam, M.A. Al-Omair, F. Ullah, Catalytic comparison of various polar Zn(II)-Schiff base complexes and VO(II)-Schiff base complexes in (ep)oxidation processes of 1,2-cyclohexene and cyclohexane, Res. Chem. Intermed., 45 (2019) 4653–4675. https://doi.org/10.1007/s11164-019-03855-8.
[47] L. Zhou, P. Cai, Y. Feng, J. Cheng, H. Xiang, J. Liu, D. Wu, X. Zhou, Synthesis and photophysical properties of water-soluble sulfonato-Salen-type Schiff bases and their applications of fluorescence sensors for Cu^{2+} in water and living cells, Anal. Chim. Acta., 735 (2012) 96–106. https://doi.org/10.1016/j.aca.2012.05.022.
[48] M.L. Ramos, L.L.G. Justino, H.D. Burrows, Structural considerations and reactivity of peroxocomplexes of V(V), Mo(VI) and W(VI), Dalton Trans., 40 (2011) 4374. https://doi.org/10.1039/c0dt01095b.
[49] L. Petrakis, Quadrupolar relaxation of aluminum-27 nuclear magnetic resonance in aluminum alkyls, J. Phys. Chem, 72 (1968) 4182–4188. https://doi.org/10.1021/j100858a041.
[50] J. W. Akitt, Multinuclear NMR, J. Mason Plenum Press, New York, 1987, 259–292.
[51] J.W. Akitt, Multinuclear studies of aluminium compounds, Progress in Nuclear Magnetic Resonance Spectroscopy, 21 (1989) 1–149.
[52] J.P. André, H.R. Mäcke, NMR spectroscopy of Group 13 metal ions: biologically relevant aspects, J. Inorg. Biochem., 97 (2003) 315–323. https://doi.org/10.1016/S0162-0134(03)00315-5.
[53] F. Venema, Coordination of Aluminium(III) with hydroxycarboxylates in water, PhD thesis, Technical University of Delft, Netherlands, 1992.
[54] C. Bae, S. Lee, S.-Y. Choi, G. Kwag, Synthesis and Characterization of Monomeric, Oligomeric, and Polymeric Aluminum 8-Hydroxyquinolines, Inorg. Chem., 44 (2005) 7911–7917. https://doi.org/10.1021/ic050920o.
[55] R. K. Jain, A. P. Mishra and P. Gupta, Thermal analyses and spectral characterization of some synthesized metal(II) Schiff base complexes, J Therm Anal Calorim., 110 (2012), 529–534. https://doi.org/10.1007/s10973-012-2401-8.
[56] S.L. Mayo, B.D. Olafson, W.A. Goddard, DREIDING: a generic force field for molecular simulations, J. Phys. Chem., 94 (1990) 8897–8909. https://doi.org/10.1021/j100389a010.
[57] MarvinSketch 15.3.2.0, 2015, ChemAxon (http://www.chemaxon.com).
[58] A.D. Becke, Density-functional exchange-energy approximation with correct asymptotic behavior, Phys. Rev. A., 38 (1988) 3098–3100. https://doi.org/10.1103/PhysRevA.38.3098.
[59] C. Lee, W. Yang, R.G. Parr, Development of the Colle-Salvetti correlation-energy formula into a functional of the electron density, Phys. Rev. B., 37 (1988) 785–789. https://doi.org/10.1103/PhysRevB.37.785.
[60] S.H. Vosko, L. Wilk, M. Nusair, Accurate spin-dependent electron liquid correlation energies for local spin density calculations: a critical analysis, Can. J. Phys., 58 (1980) 1200–1211. https://doi.org/10.1139/p80-159.
[61] M. J. Frisch, G. W. Trucks, H. B. Schlegel, G. E. Scuseria, M. A. Robb, J. R. Cheese-man, G. Scalmani, V. Barone, G. A. Petersson, H. Nakatsuji, et al., Gaussian 16, Revision B.01, Gaussian, Inc., Wallingford CT, 2016.
[62] A.D. McLean, G.S. Chandler, Contracted Gaussian basis sets for molecular calculations. I. Second row atoms, Z =11–18, J. Chem. Phys., 72 (1980) 5639–5648. https://doi.org/10.1063/1.438980.
[63] R. Krishnan, J.S. Binkley, R. Seeger, J.A. Pople, Self-consistent molecular orbital methods. XX. A basis set for correlated wave functions, J. Chem. Phys., 72 (1980) 650–654. https://doi.org/10.1063/1.438955.
[64] M.J. Frisch, J.A. Pople, J.S. Binkley, Self-consistent molecular orbital methods 25. Supplementary functions for Gaussian basis sets, J. Chem. Phys., 80 (1984) 3265–3269. https://doi.org/10.1063/1.447079.
[65] S. Miertuš, E. Scrocco, J. Tomasi, Electrostatic interaction of a solute with a continuum. A direct utilizaion of AB initio molecular potentials for the prevision of solvent effects, Chem. Phys., 55 (1981) 117–129. https://doi.org/10.1016/0301-0104(81)85090-2.
[66] J. Tomasi, B. Mennucci, R. Cammi, Quantum Mechanical Continuum Solvation Models, Chem. Rev., 105 (2005) 2999–3094. https://doi.org/10.1021/cr9904009.
[67] G. Ogruc Ildiz, J. Konarska, R. Fausto, UV-induced conformational isomerization and photochemistry of 3-chloro-4-methoxybenzaldehyde in cryogenic inert matrices, J. Chem. Phys., 151 (2019). https://doi.org/10.1063/1.5118332.
[68] L.L.G. Justino, S. Braz, M.L. Ramos, Spectroscopic and DFT Study of Alizarin Red S Complexes of Ga(III) in Semi-Aqueous Solution, Photochem., 3 (2023) 61–81. https://doi.org/10.3390/photochem3010005.
[69] L.L.G. Justino, I. Reva, R. Fausto, Thermally and vibrationally induced conformational isomerizations, infrared spectra, and photochemistry of gallic acid in low-temperature matrices, J. Chem. Phys., 145 (2016) 014304. https://doi.org/10.1063/1.4954894.

[70] F. London, Théorie quantique des courants interatomiques dans les combinaisons aromatiques, Journal de Physique et Le Radium, 8 (1937) 397–409. https://doi.org/10.1051/jphysrad:01937008010039700.
[71] R. McWeeny, Perturbation Theory for the Fock-Dirac Density Matrix, Phys. Rev., 126 (1962) 1028–1034. https://doi.org/10.1103/PhysRev.126.1028.
[72] R. Ditchfield, Self-consistent perturbation theory of diamagnetism, Mol. Phys., 27 (1974) 789–807. https://doi.org/10.1080/00268977400100711.
[73] K. Wolinski, J.F. Hinton, P. Pulay, Efficient implementation of the gauge-independent atomic orbital method for NMR chemical shift calculations, JACS, 112 (1990) 8251–8260. https://doi.org/10.1021/ja00179a005.
[74] J.R. Cheeseman, G.W. Trucks, T.A. Keith, M.J. Frisch, A comparison of models for calculating nuclear magnetic resonance shielding tensors, J. Chem. Phys., 104 (1996) 5497–5509. https://doi.org/10.1063/1.471789.
[75] J. Liu, J. Cheng, X. Ma, X. Zhou, H. Xiang, Photophysical properties and pH sensing applications of luminescent salicylaldehyde derivatives, Res. Chem. Intermed., 42 (2016) 5027–5048. https://doi.org/10.1007/s11164-015-2343-4.
[76] C.A. Hawkins, C.G. Bustillos, R. Copping, B.L. Scott, I. May, M. Nilsson, Challenging conventional f-element separation chemistry – reversing uranyl(VI)/lanthanide(III) solvent extraction selectivity, Chem. Comm., 50 (2014) 8670. https://doi.org/10.1039/C4CC03031A.